

Supplementary Materials: A macroevolutionary perspective on how dispersal can affect biodiversity and vice versa

Hagen O Viana SD Wiegand T Chase JM Onstein RE

Environment

We simulate 5 Myrs of environmental dynamics of four patches (i.e. A, B, C and D), inspired by a theoretical but realistic isolated island system placed in the South. The total area is 60X60 Km², with site area is 1 Km², time-step is 10'000 years, and 501 time-steps=(Animation 1). We consider dynamic topography, minimum temperature, and maximum temperature, combined with sea level changes which intensify during the Quaternary (~last 2.6 Ma), and happened in a periodicity of 100 ky (i.e. 10 time steps) (Pillans, Chappell, and Naish 1998). This approximates Earth's eccentricity with a conservative periodicity (Shepard et al. 2018) and reflects interactions among global climate dynamics and changes in incoming solar radiation, likely influencing ecological and evolutionary patterns. We approximate empirical mean temperature and sea levels (Westerhold et al. 2020; Hoffmann and Sgrò 2011). Our dynamic temperature oscillates at similar periodicity and temporal intensity, so that lower temperature periods match periods of lowest sea levels (*Figure 1 Main*, Figure 1). Given the random attribute location on Earth, i.e. Southern Hemisphere, the south sides of each patch were 2°C colder than the northern sides and were smoothed with a focal function of mean 3x3 sites (raster package). We derive T_{min} and T_{max} fluctuations though time decreasing 0.01°C (i.e. lapse rate 0.01°C/m) for each increase in altitude (m). We draw minimum and maximum temperature from site mean temperatures by respectively subtracting and adding the absolute values from a normal distribution with mean=0 and standard deviation $SD = \frac{E_i}{\max(E)}$. This means that the distance between T_{min} and T_{max} increases in likelihood as scaled site elevation E_i (m) increases. Lowest elevation across all times was -115m and highest elevation across all times was 803m from final time-step sea level (i.e. 0m). This resulted in temperature ranges of 0—5°C (Animation 1, Figure 1 B and D). In all our simulations we penalize connectivity though a cost multiplier of geographical distance (Hagen et al. 2021). We used a cost of four (4) for unsuitable sites (i.e. under sea level) and 1 for suitable sites with the addition of 0.1 per 100m slope difference between source and destination site (Figure 2). Empirical evidence suggests that for high elevation species, greater elevation equals greater dispersal barriers, as

mountain peaks are often embedded in a low elevation matrix, thus creating an island-like system (Vasconcelos et al. 2020). Moreover, by choosing a strong matrix resistance, i.e. four, we stress the effects of topography, geodynamics and sea-level changes considering habitat unsuitability within 10'000 years.

Our simulations started with three patches (i.e. A, B and C) which do not change in topography and end with four (i.e. A, B, C and D) patches (Figure 1). Patch A and B have their connectivity periodically increased as a result of a shallow land bridge that increases in connectivity depending on sea level changes (Figure 1 Main , Animation 1, Figure 2) while patch C remains relatively isolated. Patch D begins appearing around 1.5 Ma as a result of topographic and sea level changes (Figure 1 Main).

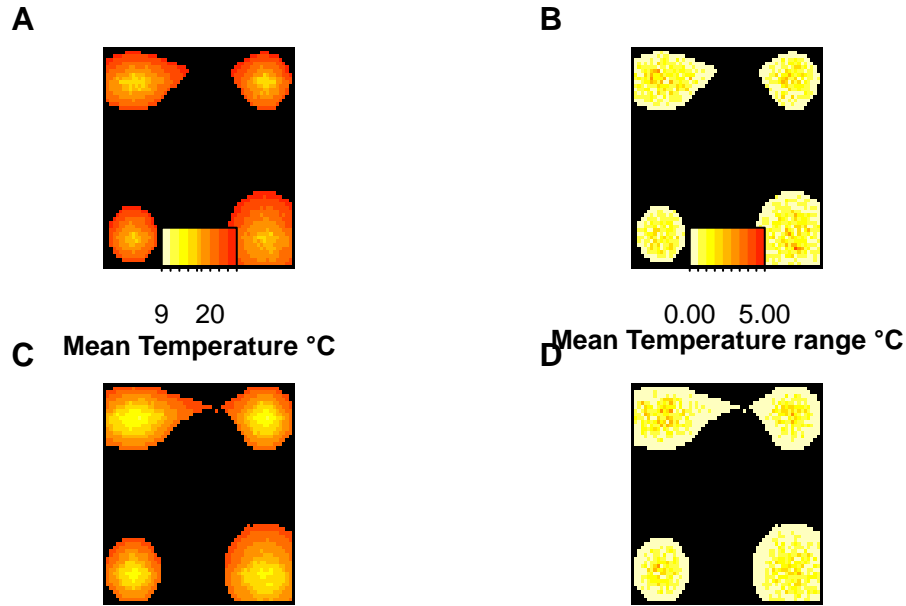


Figure 1: Mean temperature (A,C) and temperature range (i.e. $\text{max_temp} - \text{min_temp}$) (B,D) in °C for the present (A,B) and past 130'000 years (C,D). Note that periods of low sea level also correlate with mean average global temperature, since ice formations over land masses under low temperatures cause sea level drops. On the other hand, temperature and temperature ranges correlate with elevation. Final temperature is the mean average global temperature with a decrease in temperature with elevation and a slight increase in temperature if sites are facing North. Differences between minimal and maximal temperatures were higher the higher the elevation, reflecting stronger temperature temporal variability at higher elevation sites.

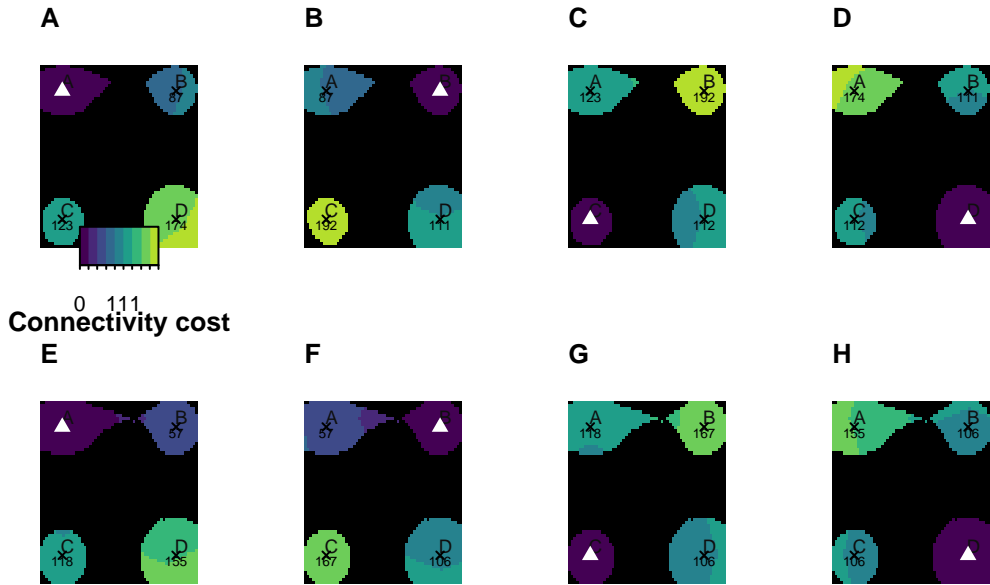


Figure 2: Connectivity costs in reference to the center of each patch (i.e. A,B,C and D) for two time steps, i.e. Present (0 Ma, resp. A,B,C and D) and for 130'000 years ago (0.13 Ma, resp. E,F,G and H). Note the changes in connectivity due to sea level changes between the present and the lowest seal level period (i.e. 0.13 Ma). Numbers shown are resistance x geographical distance from the source (white triangle) to the centre of each patch (crosses).

Eco-evolutionary models

All models, i.e. M0, ME and MET, were initiated at 5 Ma with three species, each with populations spread through the suitable sites of each patch (i.e. sp1 on patch A, sp2 on patch B, and sp3 on patch C). Initial populations had niche width $\omega_i = 0.4$ and temperature niche optima equal to the local mean temperature $T_i = T_{mean}$. In short, M0 assumes a fixed dispersal and competitive traits for all species within a simulation ($n=2000$). ME breaks this assumption by allowing dispersal and competitive traits to evolve freely, thus diverging with time between species ($n=2000$). MET adds a zero sum (i.e. a trade-off) between dispersal and competitive traits, assuming that no super species (i.e. $d_i = 1$, $l_i = 1$) are possible ($n=2000$). M0 serves as a reference and allows the exploration of parameter ranges and sensitivity in the system. The two alternative simulation scenarios (i.e. ME and MET), referred to as counterfactuals, investigate the effects of manipulating different components of the model. Specifically, these counterfactuals involve modifying the underlying biological model referring to the evolution and trade-offs between dispersal and competitive abilities, focusing on how dispersal and species interactions affect colonization and other emergent properties in our eco-evolutionary models.

This automatically made species within a simulation not only diverge between each other on their temperature optime T_i and niche widht ω_i (i.e. for M0, ME and MET), but also on dispersal d_i and competitive l_i traits (i.e. for ME and MET). For each model, we ran 2000 simulations with the same parameters. This systematic exploration of alternative scenarios allowed us to assess the impact of specific model parameters on the resulting biodiversity patterns. Specifically, we collected α , β and γ biodiversity metrics, colonization, speciation, extinction as well as trait proxies related to environmental and biotic suitability.

Frequencies of dispersal are given according to a Weibull function that has scale changed between $\phi = 1 - 50$ and shape $\Psi = 2$. Dispersal ability value d scales ϕ , resulting in concentrated short range dispersal events for small dispersal values d with increasingly larger and longer tails for larger d Figure 3. A dispersal event is considered successful when a value (Figure 3) is equal or smaller than the site-site distance (Figure 2). The presence of competitors and species niche suitability can affect species distribution, and thus, their population's connectivity.

Ecological equilibrium

Ecological equilibrium was assumed for every site and for every time-step. Environmental fitness considered min and max temperature. Biomass B_i changes according to local site conditions (i.e. T_{min}, T_{max} [9—26°C]) and evolving species temperature optimum T_i and niche width ω_i according to the geometric mean of a Gaussian environmental function at minimum and maximum site temperature (for an example, see Figure 4).

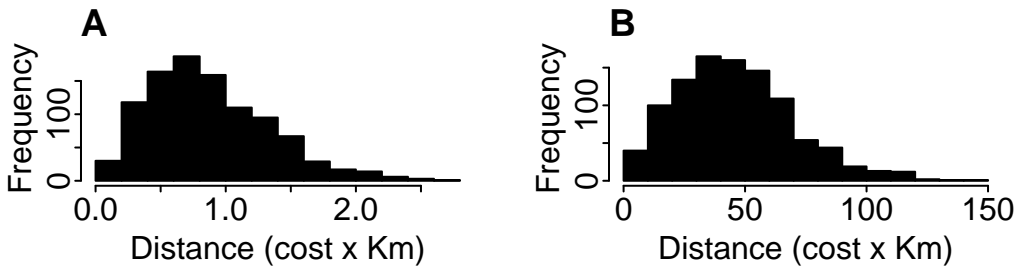


Figure 3: Histogram showing two extreme frequencies of 1000 dispersal events in a weibull distribution with shape of 2 and scale of 1 (A) and 50 (B). Note the different of the x axis.

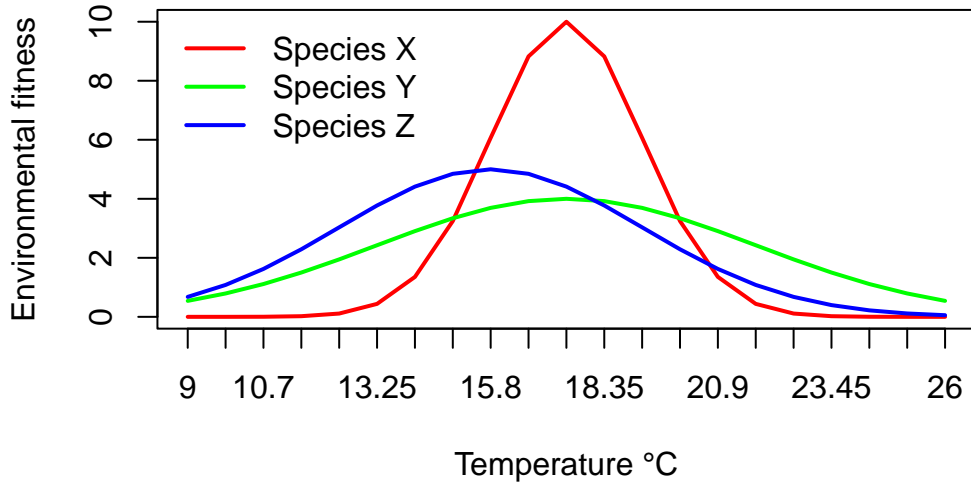


Figure 4: Environmental fitness across a temperature gradient in °C for three different species with varrying mean temperature (T) amd niche width (ω) traits. Species X (dark red) has $T=18^{\circ}\text{C}$ and $\omega=0.1$; Species Y (green) has $T=18$ and $\omega=0.25$; Species Z (blue) has $T=16$ and $\omega=0.2$. Temperature-dependent growth of biomass is applied a constant and equal rate to all simulations. Maximal growth is proportional to the geometric mean of the fitness of the focal species at the minimal and maximal temperature in the site.

Relative biomass growth rate decreased linearly with conspecific biomass B_i in the site with a conspecific interaction coefficient α_{ff} and a heterospecific interaction coefficient α_{fh} . The conspecific interaction coefficient was fixed for all simulations (i.e. $\alpha_{ff} = 0.2$), since our focus was on components on intraspecific competition, i.e. modulated through heterospecific tolerance trait (l). For an example, see the interactions between three (3) and thirteen (13) species though ODE (i.e. 30 interaction) in our Lotka-Volterra model type (Figure 5 AB and C respectively).

To estimate equilibrium in the context of competition dynamics, we implement an iterative approach. Firstly, all species in a site are checked to determine if $a_{ff} > a_{fh}$ (condition 1, eq. 8). If not, the species is removed as conspecifics are weaker competitors than heterospecifics. Next, the carrying capacity (J^*) is estimated based on the values of K_f, a_{ff}, a_{fh} for each species f (eq. 10). Then, all species are checked again to see if the product of the intraspecific competition coefficient and carrying capacity is greater than the product of the interspecific competition coefficient $a_{ff}K > a_{fh}J^*$ (condition 2, eq. 8). Species that do not meet this condition, indicating a too low carrying capacity, are removed, and the estimation process returns estimating J^* (eq. 10). This is repeated until all remaining species satisfy the condition 2. Finally, the equilibrium biomass of each species B_f^* is demonstrated using equation 8 (Figure 5).

In the special case where the interaction coefficients are the same for all species, we can derive a more detailed condition for the carrying capacity K_f required for positive abundances. In this case the total biomass J^* of the community in equilibrium can be estimated as

$$J^* = \frac{S \frac{\alpha_{ff}}{\alpha_{ff} - \alpha_{fh}}}{(1 + S \frac{\alpha_{fh}}{\alpha_{ff} - \alpha_{fh}})} \times \frac{1}{S} \sum_{f=1}^S K_f$$

Thus

$$J^* = \frac{S\alpha_{ff}}{(\alpha_{ff} + (S-1)\alpha_{fh})} \times \frac{1}{S} \sum_{f=1}^S K_f$$

and the condition $\frac{\alpha_{fh}J^*}{\alpha_{ff}K_{ff}} < 1$ becomes

$$\frac{S\alpha_{fh}}{\alpha_{ff} + (S-1)\alpha_{fh}} \times \frac{1}{S} \sum_{f=1}^S K_f$$

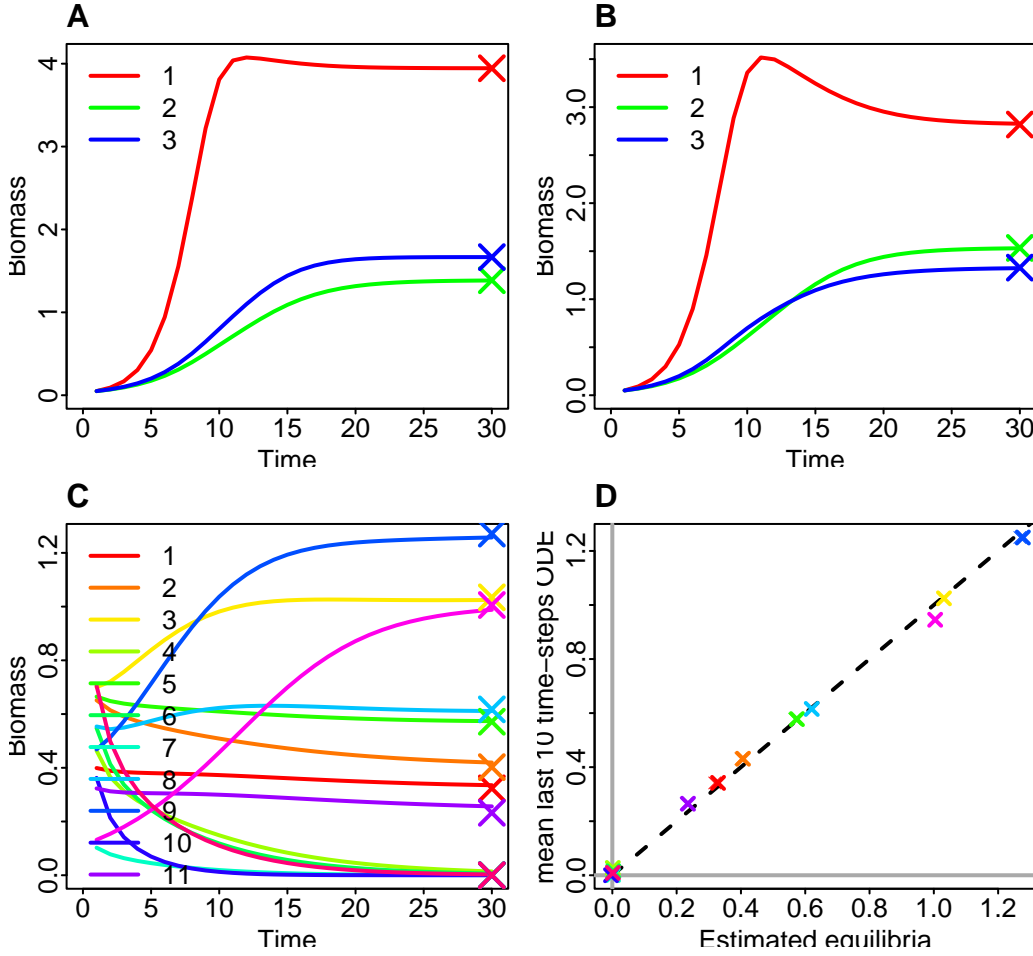


Figure 5: Local dynamics over 10'000 years showing biomass changes for different communities (ABC) and comparison of mean last 10 time-steps of the ODE against estimated equilibria (D). Crosses indicate the estimated ecological equilibria. (A) Species 1 and 2, have a mean temperature closer to site conditions than species 3. Moreover, species 1, 2 and 3 have niche widths of $\omega_1 = 0.1, \omega_2 = 0.25, \omega_3 = 0.2$ and the same heterospecific tolerance ($l=0.98$). (B) we change heterospecific tolerance to ($l_1 = 0.9, l_2 = 0.98, l_3 = 0.96$). (C) Random community of 13 species. (D) Comparison of mean last 10 time-steps of ODE of community in (C) against estimated equilibria; grey lines show zero lines and dashed line show the 1-1 line. Note that we use here only 30 interactions though time and we increase in precision by increasing the number of interactions (ODE time-steps) and decreasing the number of coexisting species.

Initial conditions

We did a full factorial experiment considering the full range of dispersal and competitive abilities $d_i = [0-1]$ $l_i = [0.9-1]$ and fixed $\Theta_s = 65$ (Figure 6). For model MET we impose the trade-off to the same parameters as in the other models, to ensure that initial species conform to the assumptions of MET. We randomized the seed at this stage, so that each single simulation could be reproduced.

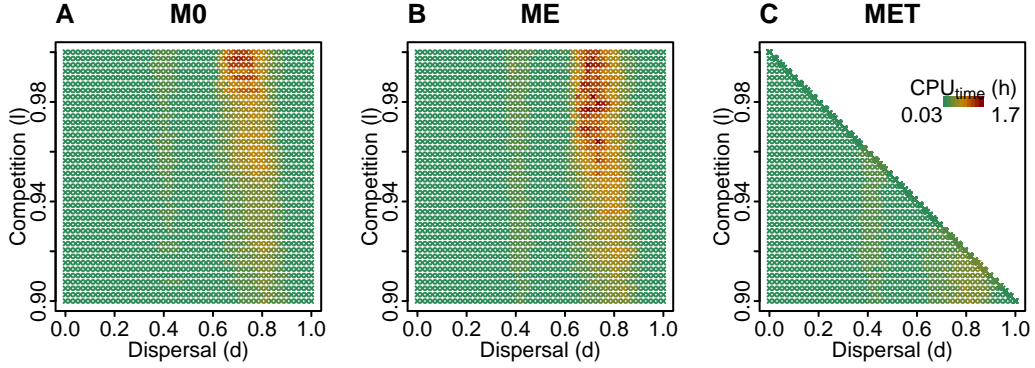


Figure 6: Initial competition and dispersal parameters for the main models and experiments. Colors show the CPU time per simulation ($n=6000$).

Results

M0 diversity statistics reflected our expectations on general patterns of diversity, such as highest speciation rates at intermediate dispersal levels (Figure 7), meaning that peaks of γ diversity relate to the spatial structure of our landscape. After investigation, all speciation events of simulations with dispersal $d_i < 0.1$ happened within patches, and mostly during the dynamic phase (Figure 15 A). Speciation within patches was only observed in M0, as for ME and MET dispersal quickly evolved beyond the critical and small dispersal distances. The qualitative changes in speciation events for intermediary dispersal $d_i = [0.15 - 0.55]$ began involving speciation events between patches C and D, but for patch D this occurred only at the dynamic time phase, i.e. 2–0 Ma (Figure 15 C).

Investigating spatial dynamics for M0 during 45-0Ma (Figure 16 A-D) showed that mean range increased with dispersal, while proportional change (i.e. $\frac{(increase-decrease)}{totalrange}$) decreased with competition. Models without interspecific competition had higher proportional increase/decrease ratio. Moreover, this signature was stronger during the dynamic stage of this simulations (Figure 16 I-L).

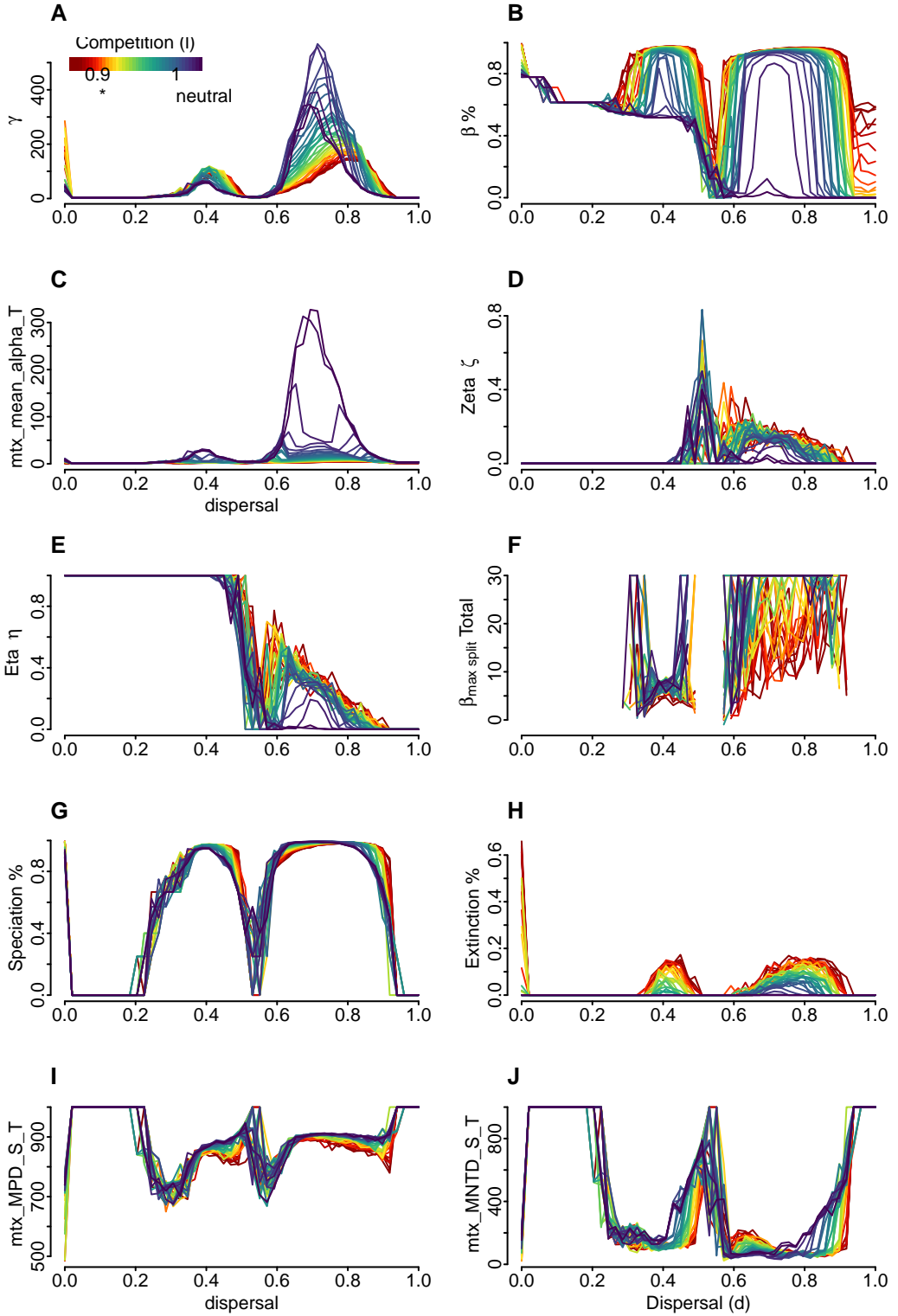


Figure 7: Summary statistics for M0 though dispersal. Each line corresponds to simulation within a same competitive value along dispersal ability.

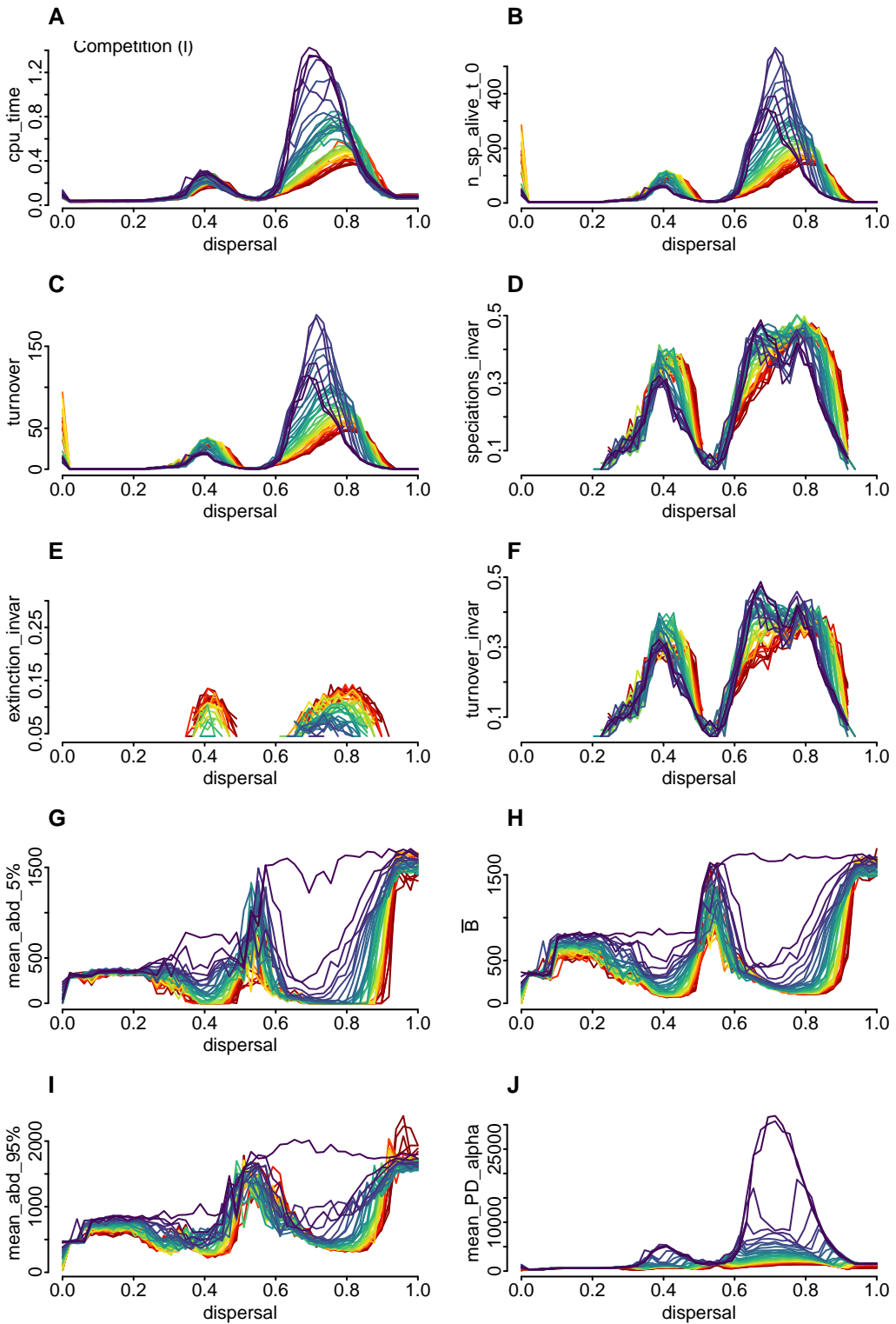


Figure 8: Additional summary statistics for M0 though dispersal. Each line corresponds to simulation within a same competitive value along dispersal ability.

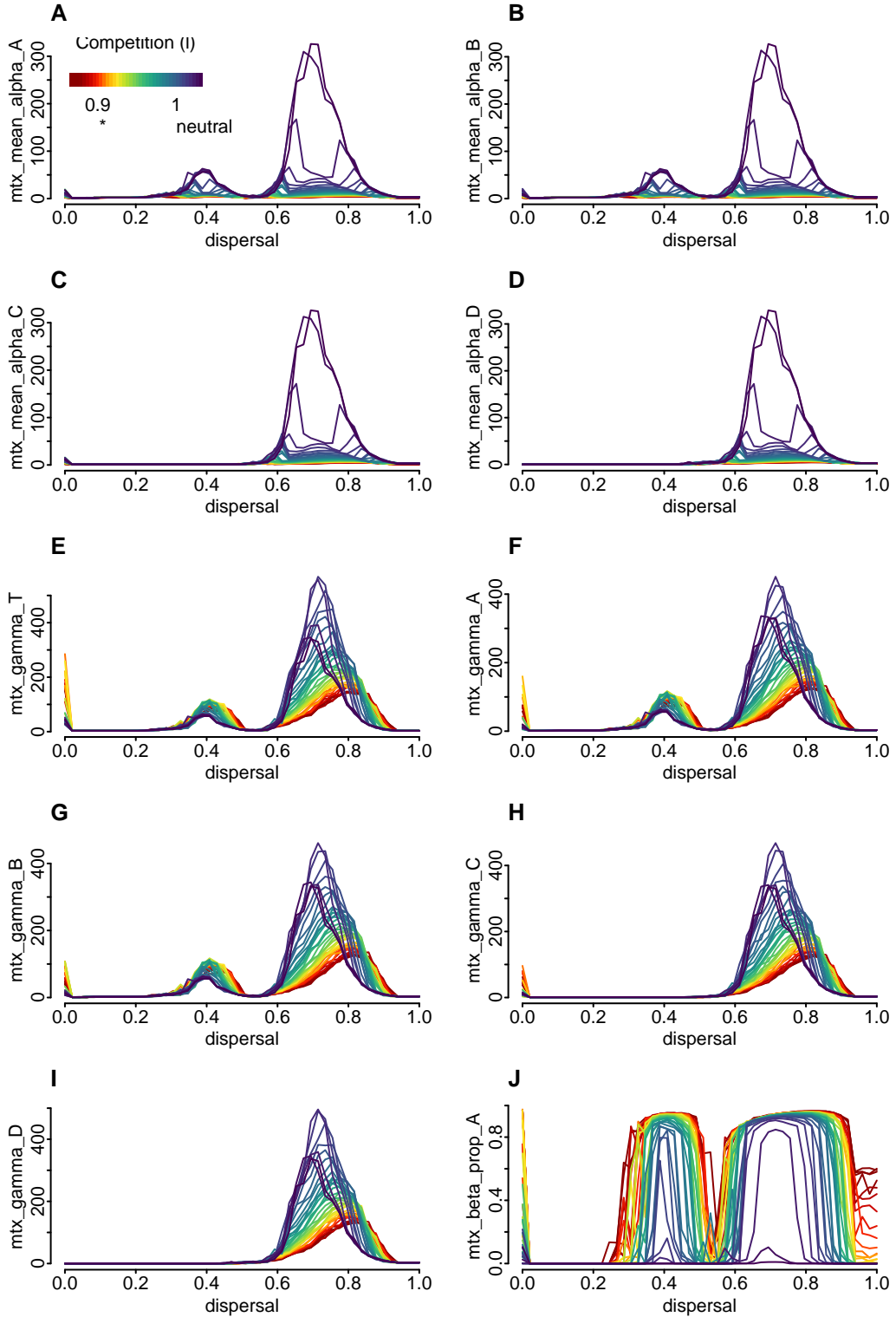


Figure 9: Additional summary statistics for M0 though dispersal. Each line corresponds to simulation within a same competitive value along dispersal ability.

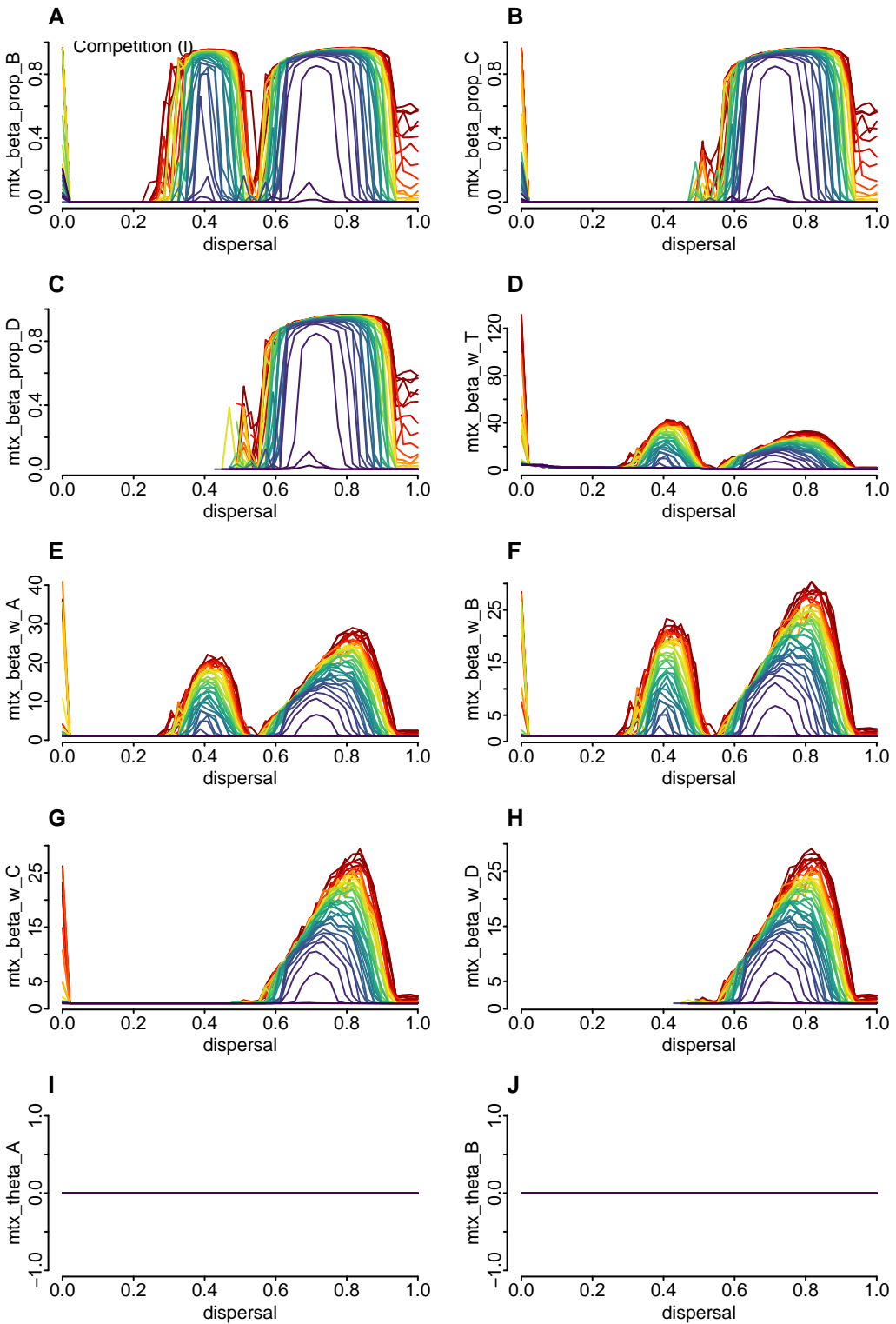


Figure 10: Additional summary statistics for M0 though dispersal. Each line corresponds to simulation within a same competitive value along dispersal ability.

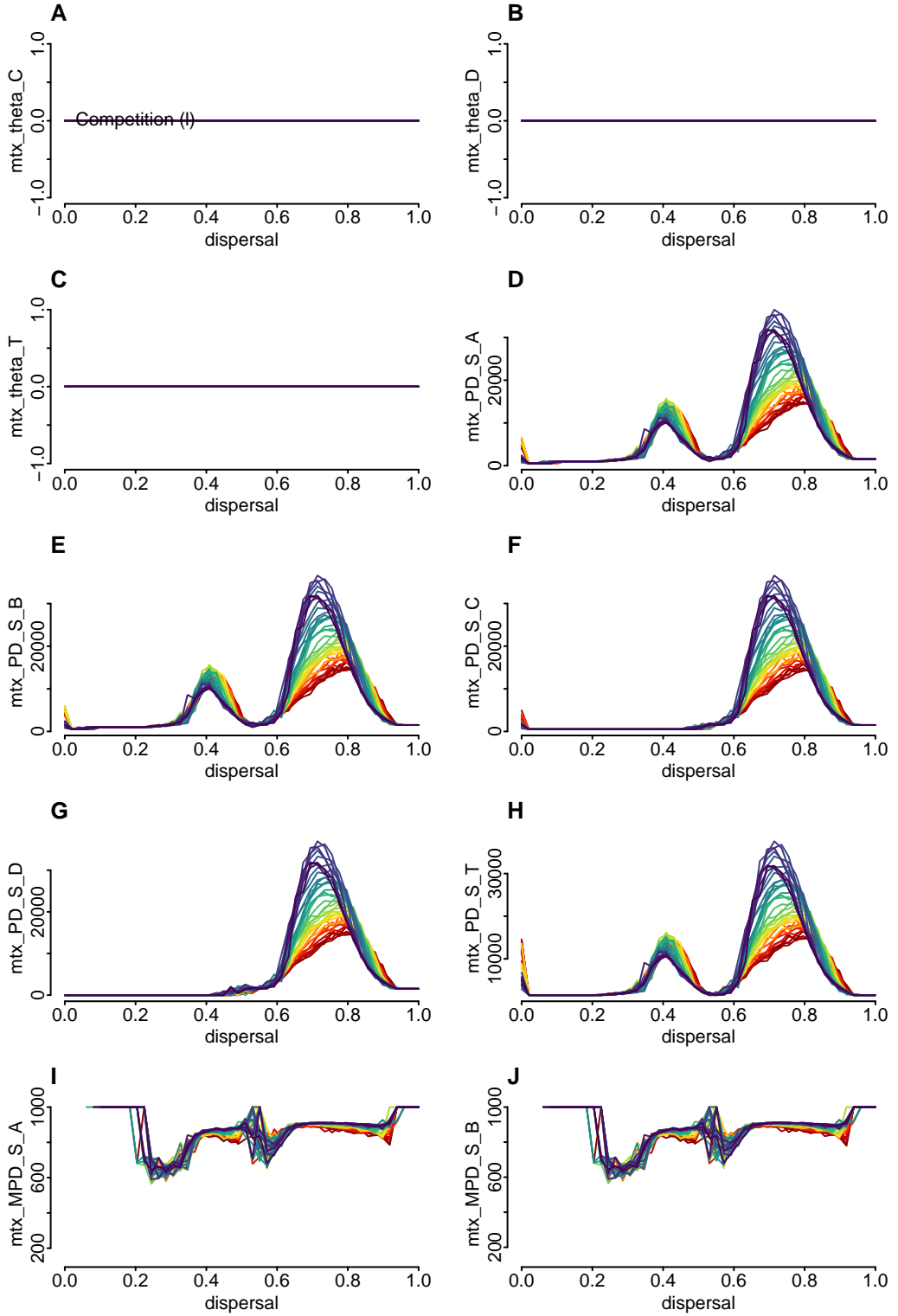


Figure 11: Additional summary statistics for M0 though dispersal. Each line corresponds to simulation within a same competitive value along dispersal ability.

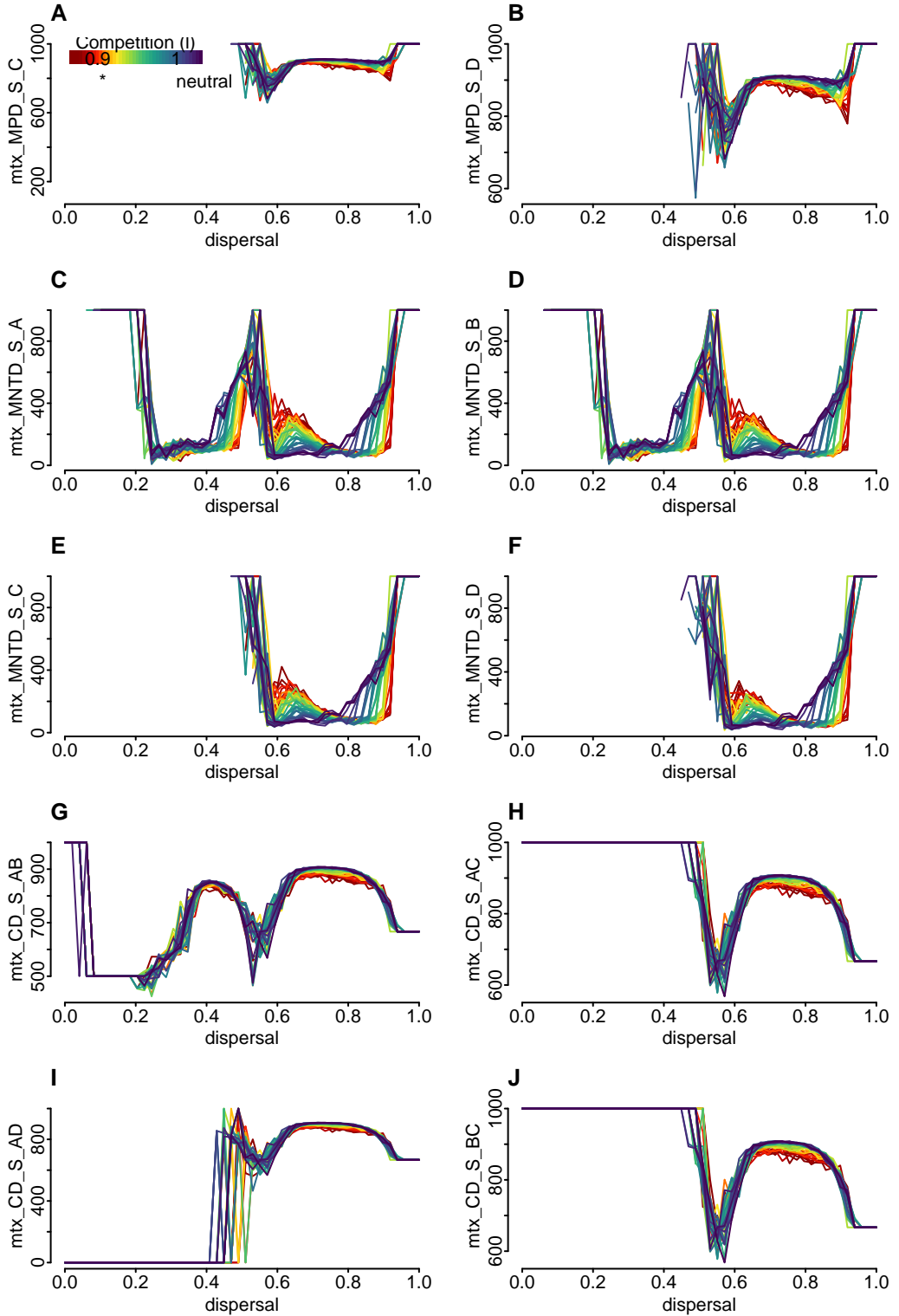


Figure 12: Additional summary statistics for M0 though dispersal. Each line corresponds to simulation within a same competitive value along dispersal ability.

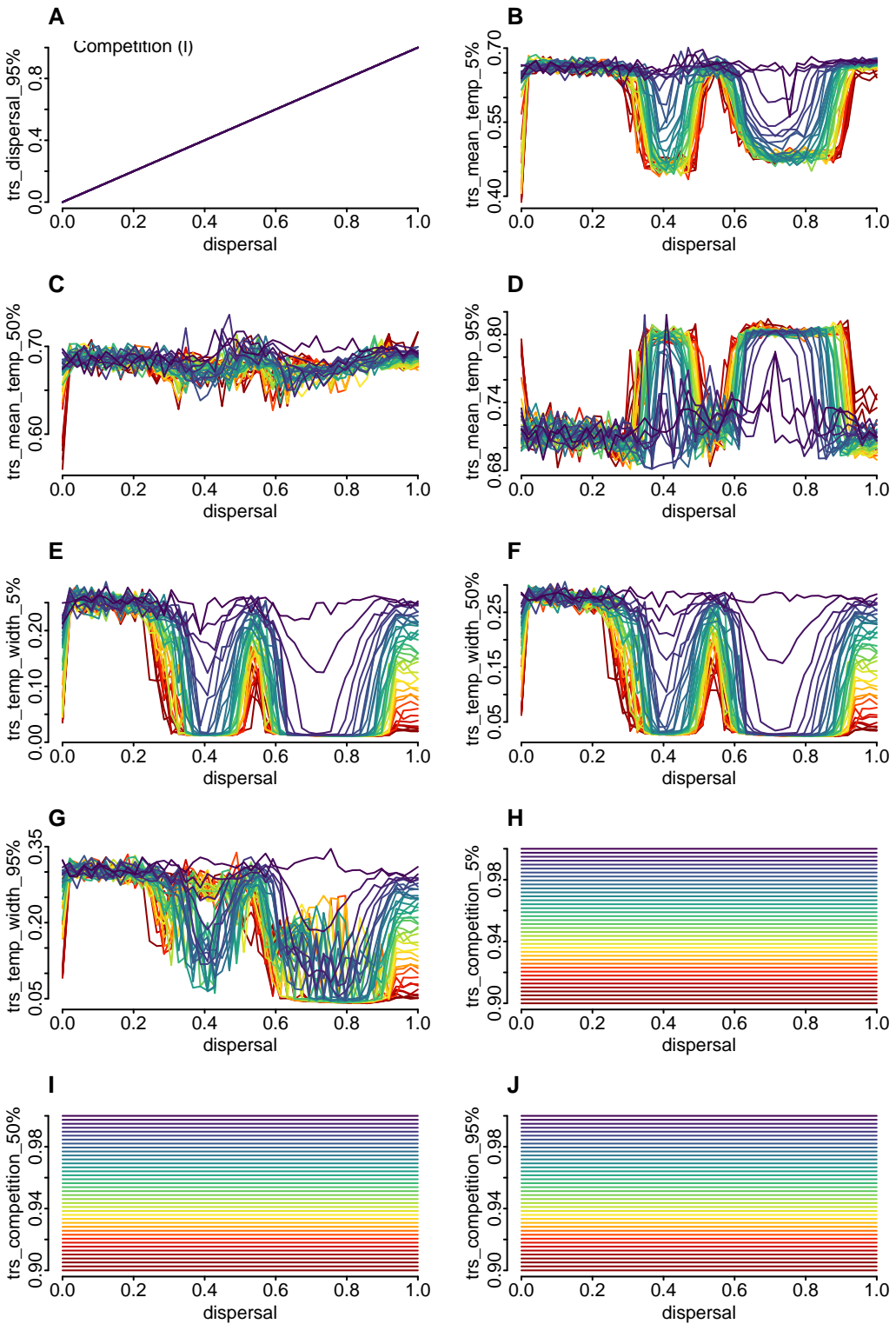


Figure 13: Additional summary statistics for M0 though dispersal. Each line corresponds to simulation within a same competitive value along dispersal ability.

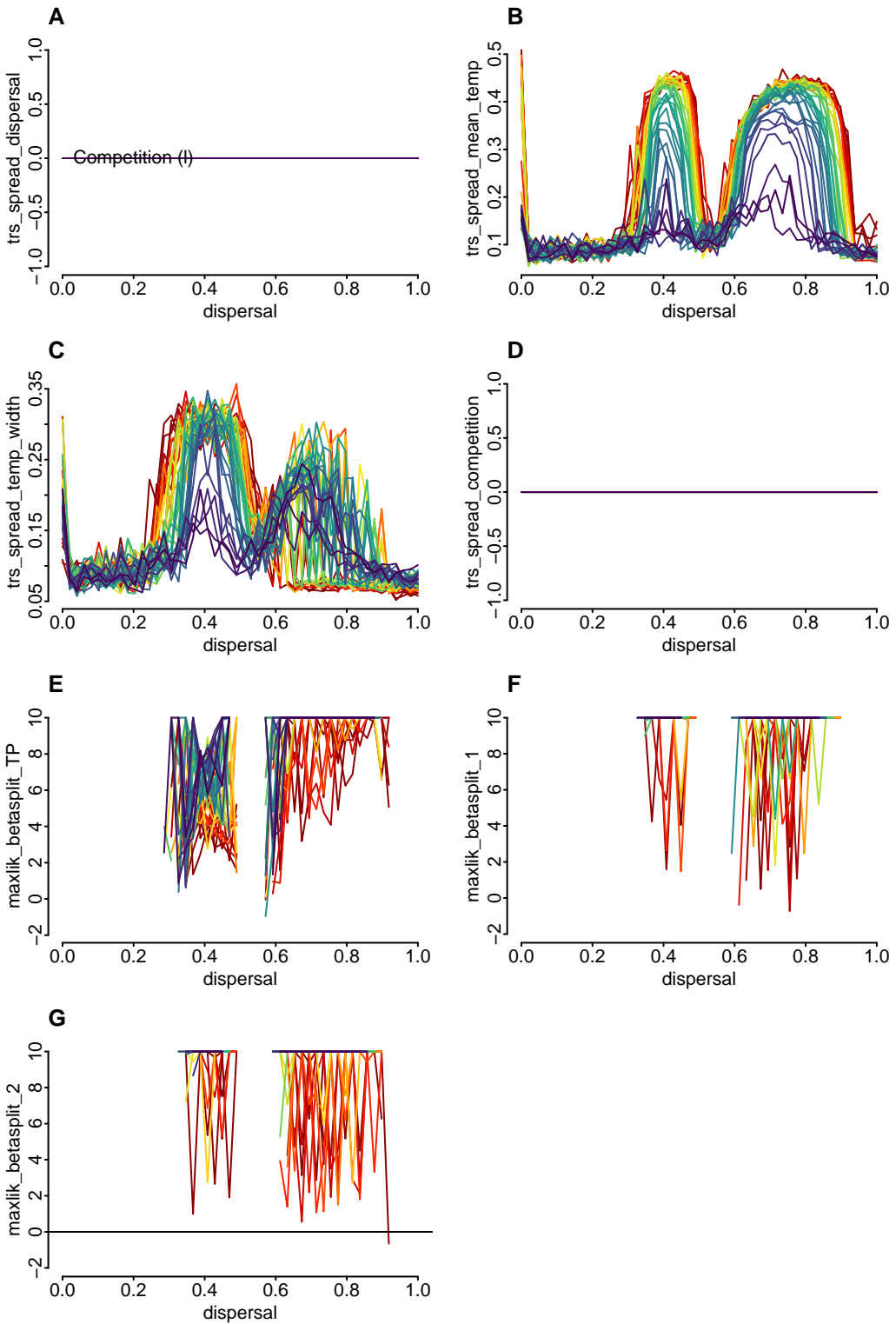


Figure 14: Additional summary statistics for M0 though dispersal. Each line corresponds to simulation within a same competitive value along dispersal ability.

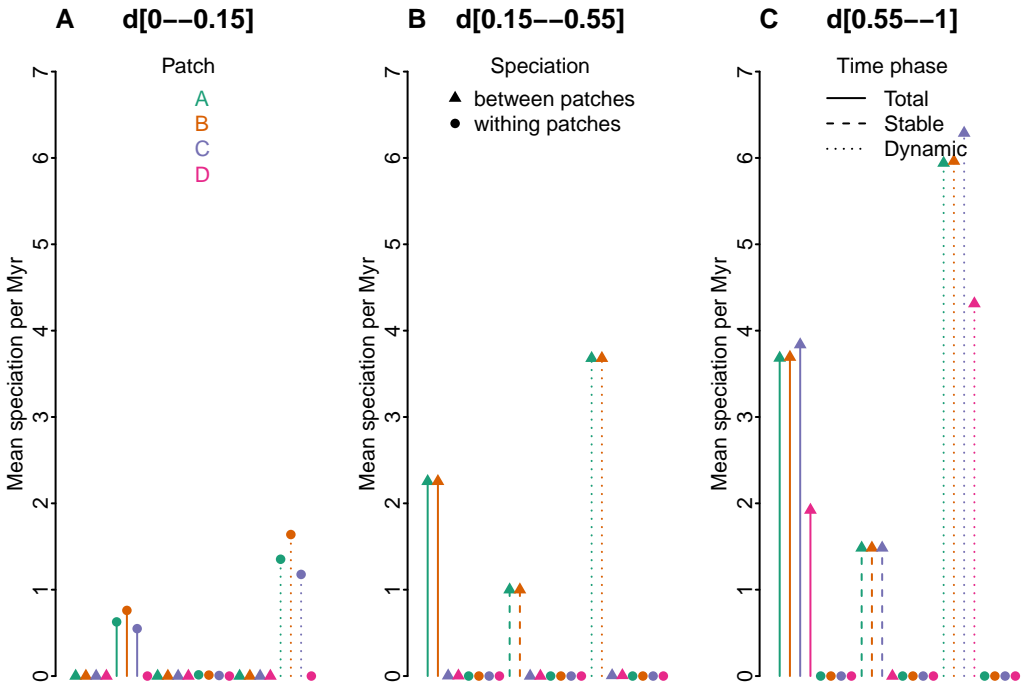


Figure 15: Mean speciation percentage for M0 with dispersal (A) smaller than 0.15; (B) between 0.15 and 0.55; and (C) bigger than 0.55. We show for each patch (in different colors) and each phase (i.e. Total 4.5-0Ma, Stable 4.5-2.5Ma, Dynamic 2-0Ma) for speciation events between or within patches (respectively triangles and circles).

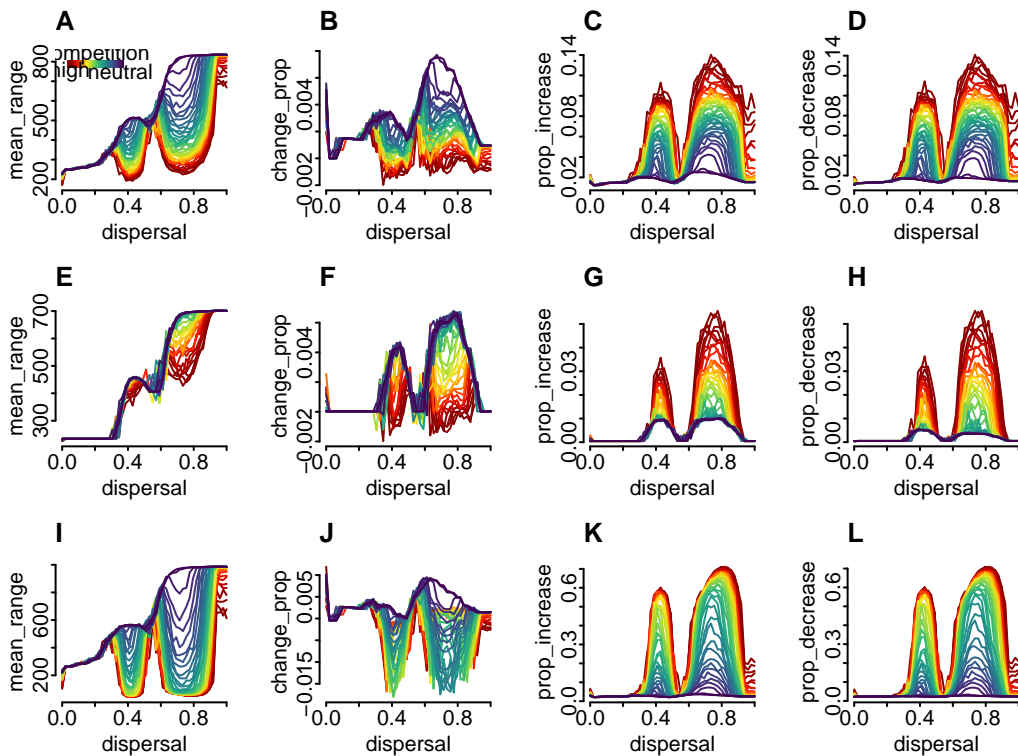


Figure 16: Spatial dynamics for M0 during Total 4.5-0Ma (A-D), Stable 4.5-2.5Ma (E-H), Dynamic 2-0Ma (I-L).

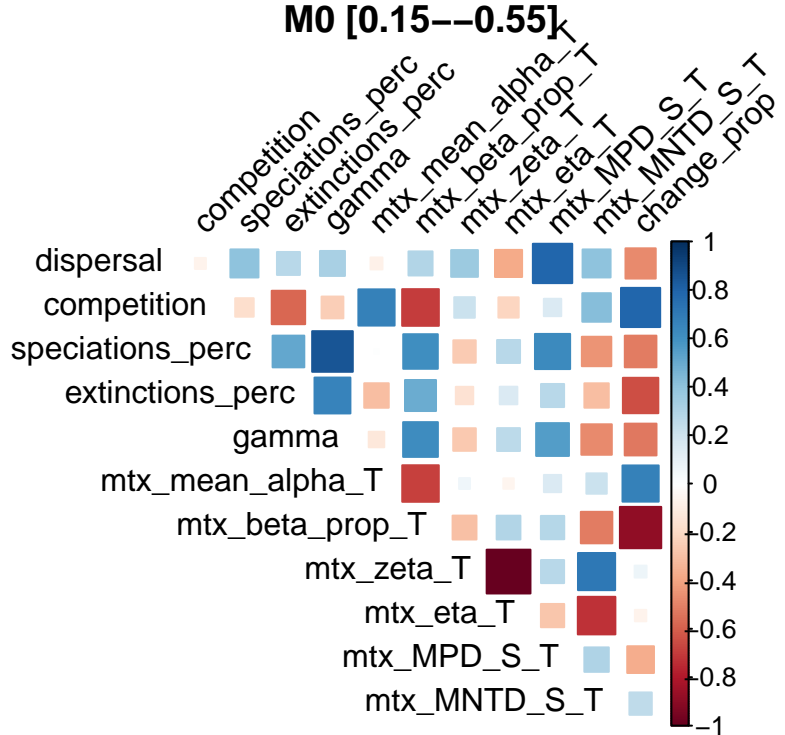
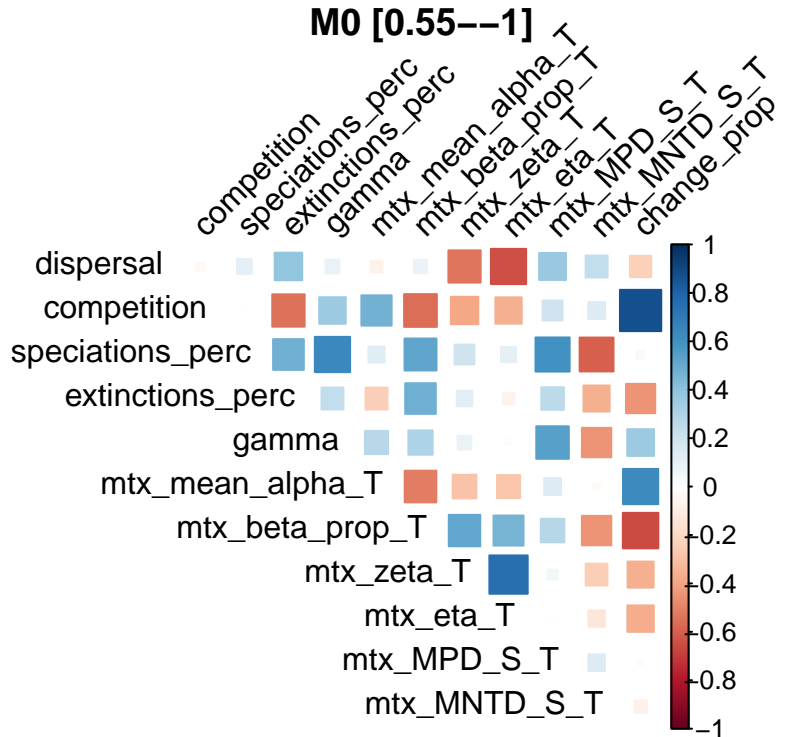
A**B**

Figure 17: Correlations for hand-picked summary statistics for M0 for different intervals of dispersal distance 0.3-0.5 (A), ; ME (B) and MET (C).

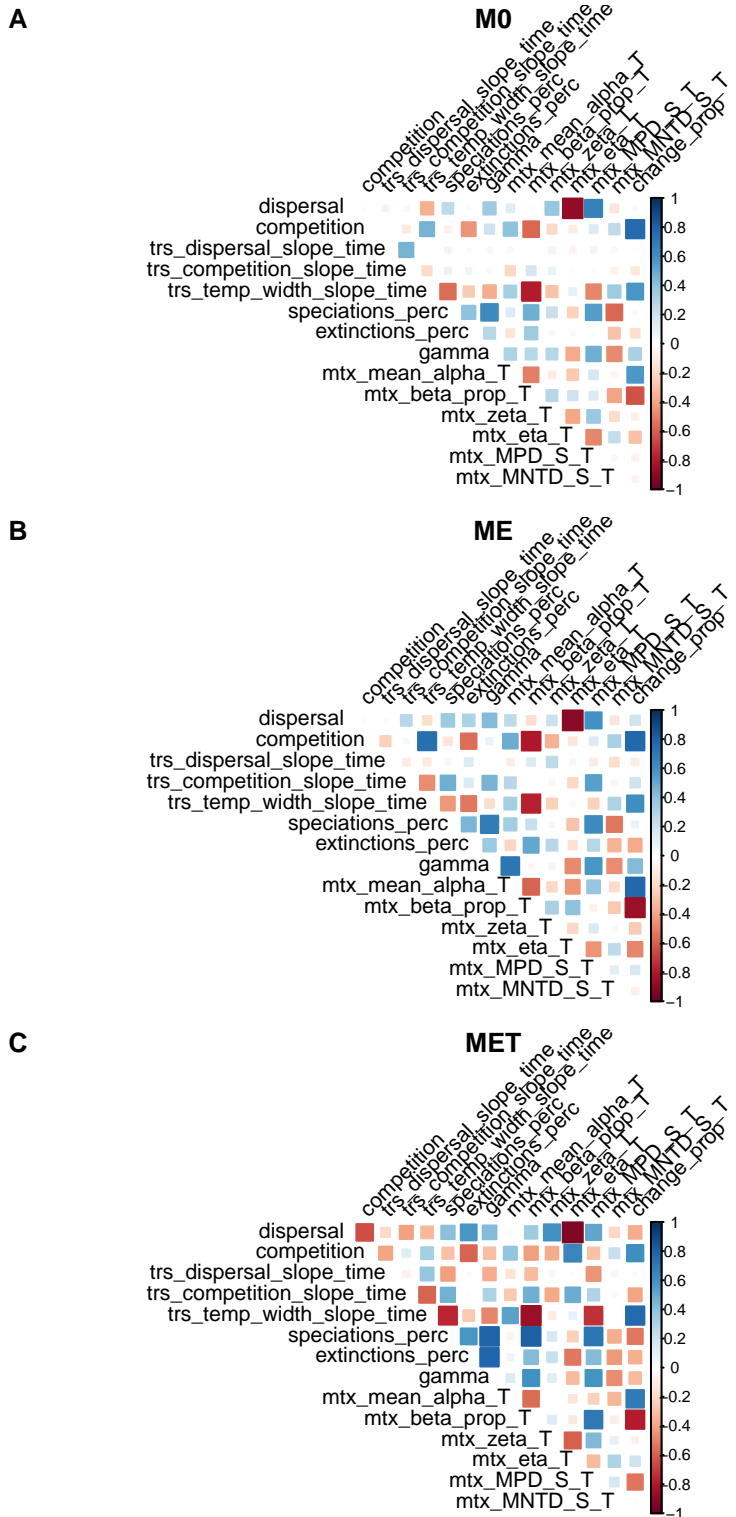


Figure 18: Correlations for hand-picked summary statistics for M0 (A); ME (B) and MET (C).

Inspecting the community distances between all the patches revealed a clear effect of increases in community diversity with patch distance and dispersal ability Figure 19 . As expected, competition tended to decrease community distance overall where communities reached maximum diversity.

Model Comparison

Beyond comparing dispersal and interspecific competition gradients between models, i.e. M0 (Figure 7, Figure 19, Figure 12 Figure 9 Figure 10 Figure 14 Figure 13 Figure 8 Figure 11), ME (Figure 28 Figure 20 Figure 21) and MET (Figure 29 Figure 22 Figure 23); we compared multiple summary statistics between models (Figure 25@fig-model-comp-patch-D).

We display here several biodiversity patterns across the three different models. For this we used multiple packages. Exploring dynamics within simulation 1119 and between models ME and MET highlight the interplay of eco-evolutionary dynamics (Figure 31). Specially, in this simulation we cover the dynamics happening at the initial peak of the dispersal regime ($d=0.37$), i.e. between patches A and B. In order to investigate a gradient of different intraspecific competition (moderated over the heterospecific tolerance trait l) we compare two simulations at the middle of first and second peak (Figure 32).

References

- Hagen, Oskar, Benjamin Flück, Fabian Fopp, Juliano S. Cabral, Florian Hartig, Mikael Pontarp, Thiago F. Rangel, and Loïc Pellissier. 2021. “Gen3sis: A General Engine for Eco-Evolutionary Simulations of the Processes That Shape Earth’s Biodiversity.” *PLoS Biology* 19 (7): e3001340. <https://doi.org/10.1371/journal.pbio.3001340>.
- Hoffmann, Ary A., and Carla M. Sgrò. 2011. “Climate Change and Evolutionary Adaptation.” *Nature* 470 (7335): 479–85. <https://doi.org/10.1038/nature09670>.
- Pillans, Brad, John Chappell, and Tim R. Naish. 1998. “A Review of the Milankovitch Climatic Beat: Template for Plio–Pleistocene Sea-Level Changes and Sequence Stratigraphy.” *Sedimentary Geology* 122 (1-4): 5–21. [https://doi.org/10.1016/S0037-0738\(98\)00095-5](https://doi.org/10.1016/S0037-0738(98)00095-5).
- Shepard, Christopher, Jon D. Pelletier, Marcel G. Schaap, and Craig Rasmussen. 2018. “Signatures of Obliquity and Eccentricity in Soil Chronosequences.” *Geophysical Research Letters* 45 (20): 11, 147–11, 153. <https://doi.org/10.1029/2018GL078583>.
- Vasconcelos, T. N. C., S. Alcantara, C. O. Andrino, F. Forest, M. Reginato, M. F. Simon, and J. R. Pirani. 2020. “Fast Diversification Through a Mosaic of Evolutionary Histories Characterizes the Endemic Flora of Ancient Neotropical Mountains.” *Proceedings of the Royal Society B: Biological Sciences* 287 (1923): 20192933. <https://doi.org/10.1098/rspb.2019.2933>.
- Westerhold, Thomas, Norbert Marwan, Anna Joy Drury, Diederik Liebrand, Claudia Agnini, Eleni Anagnostou, James S. K. Barnet, et al. 2020. “An Astronomically Dated Record of

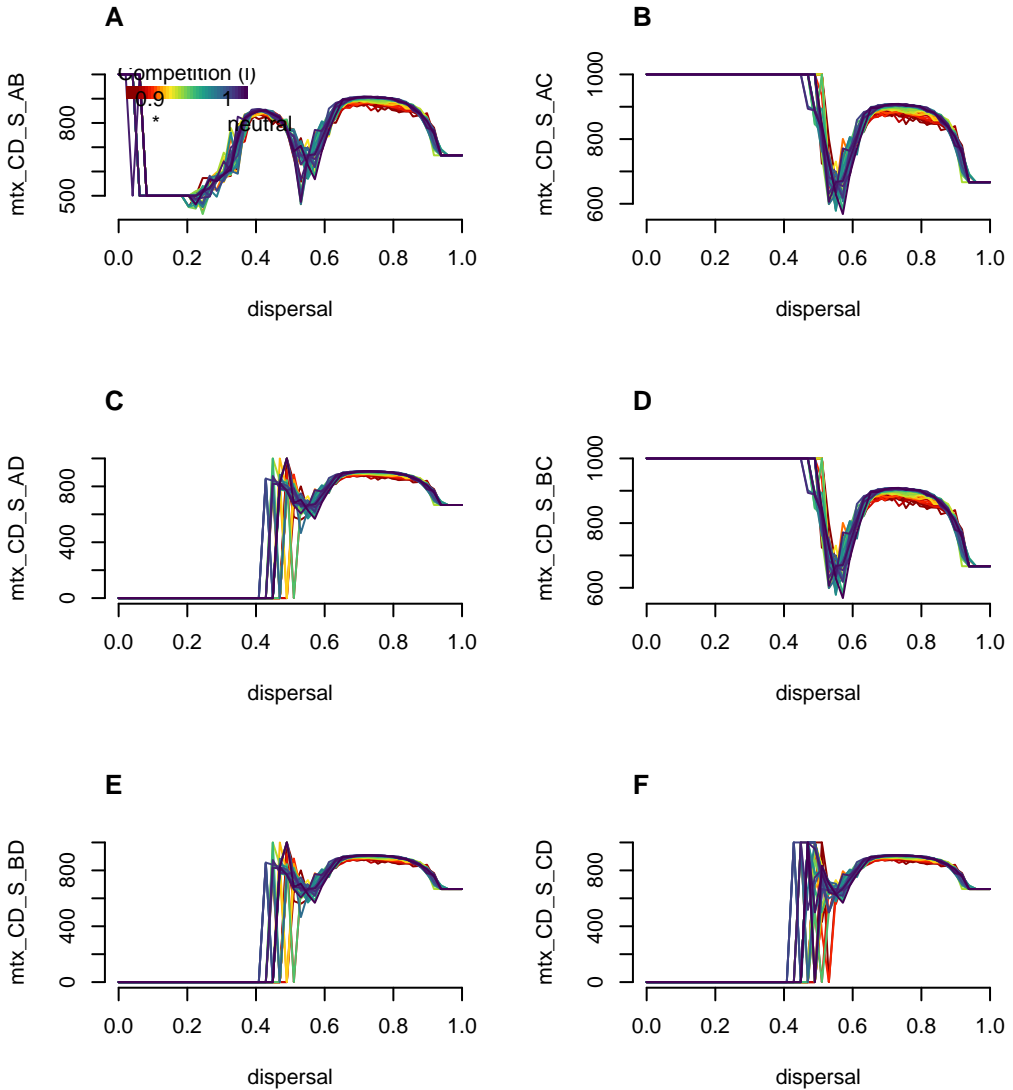


Figure 19: Community Distance between patches A, B, C and D for M0. Each line corresponds to simulations with a same competitive value.

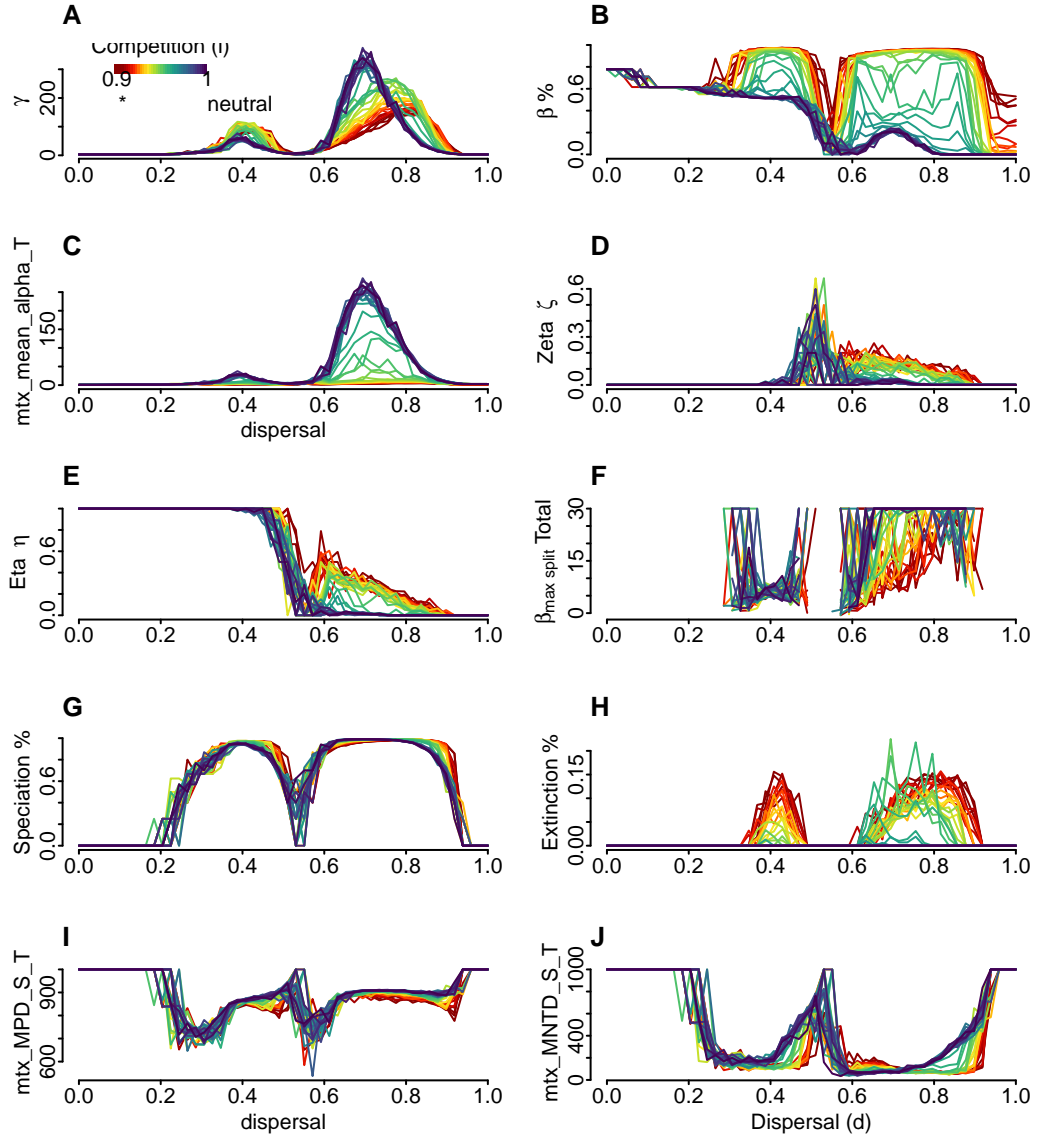


Figure 20: Summary statistics for ME through dispersal. Each line corresponds to simulation within a same competitive value along dispersal ability.

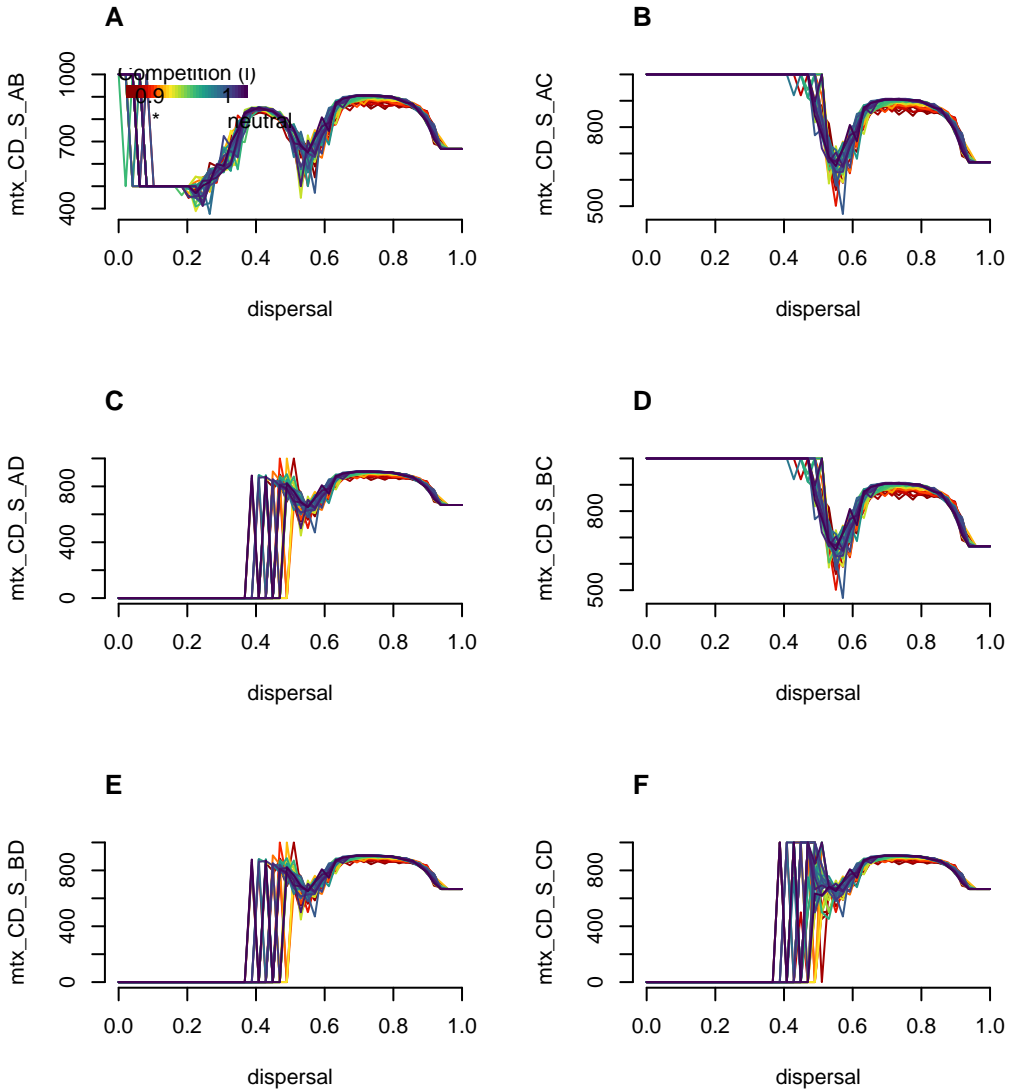


Figure 21: Community Distance between patches A, B, C and D for M0. Each line corresponds to simulations with a same competitive value.

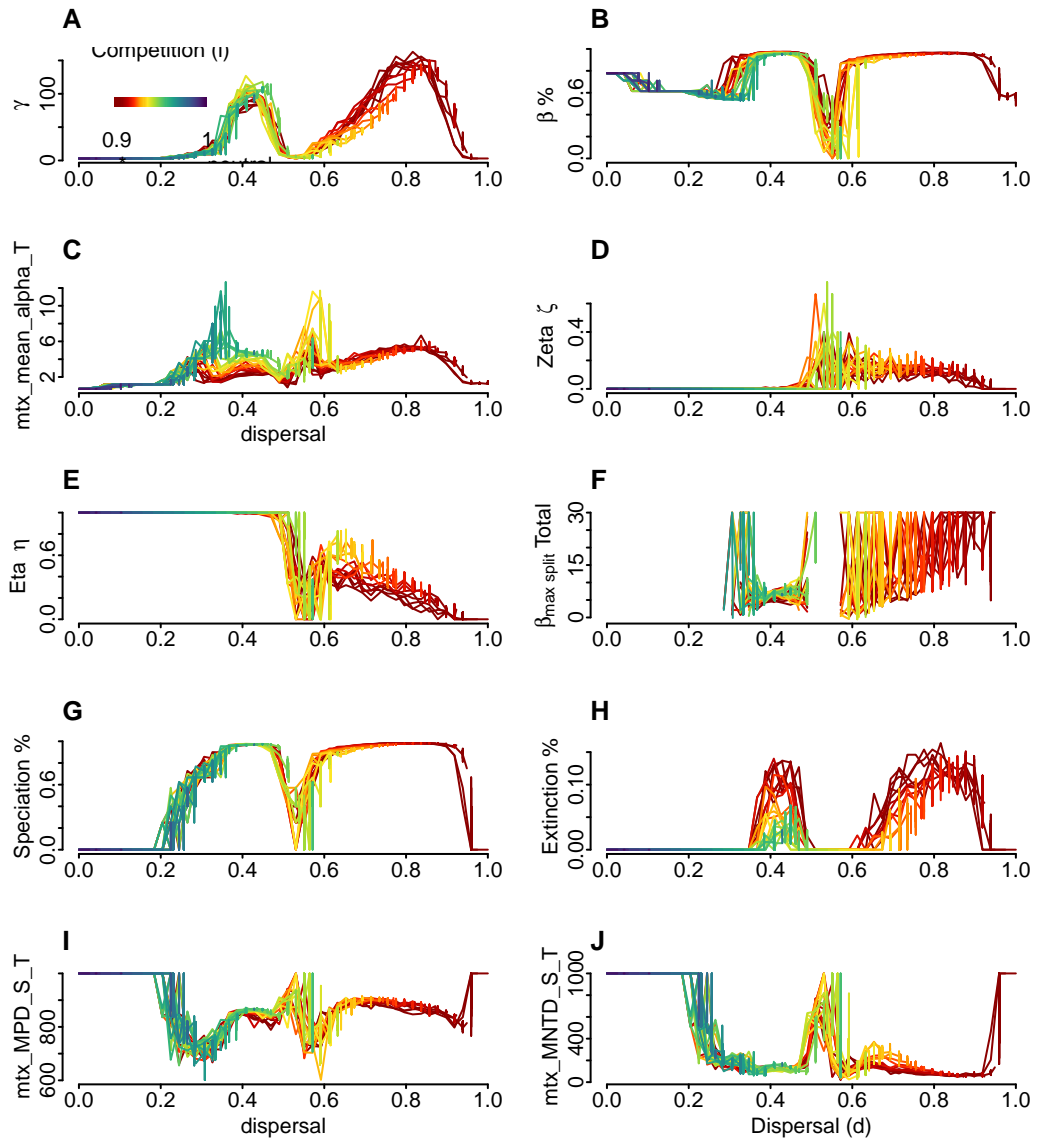


Figure 22: Summary statistics for MET through dispersal. Each line corresponds to simulation within a same competitive value along dispersal ability.

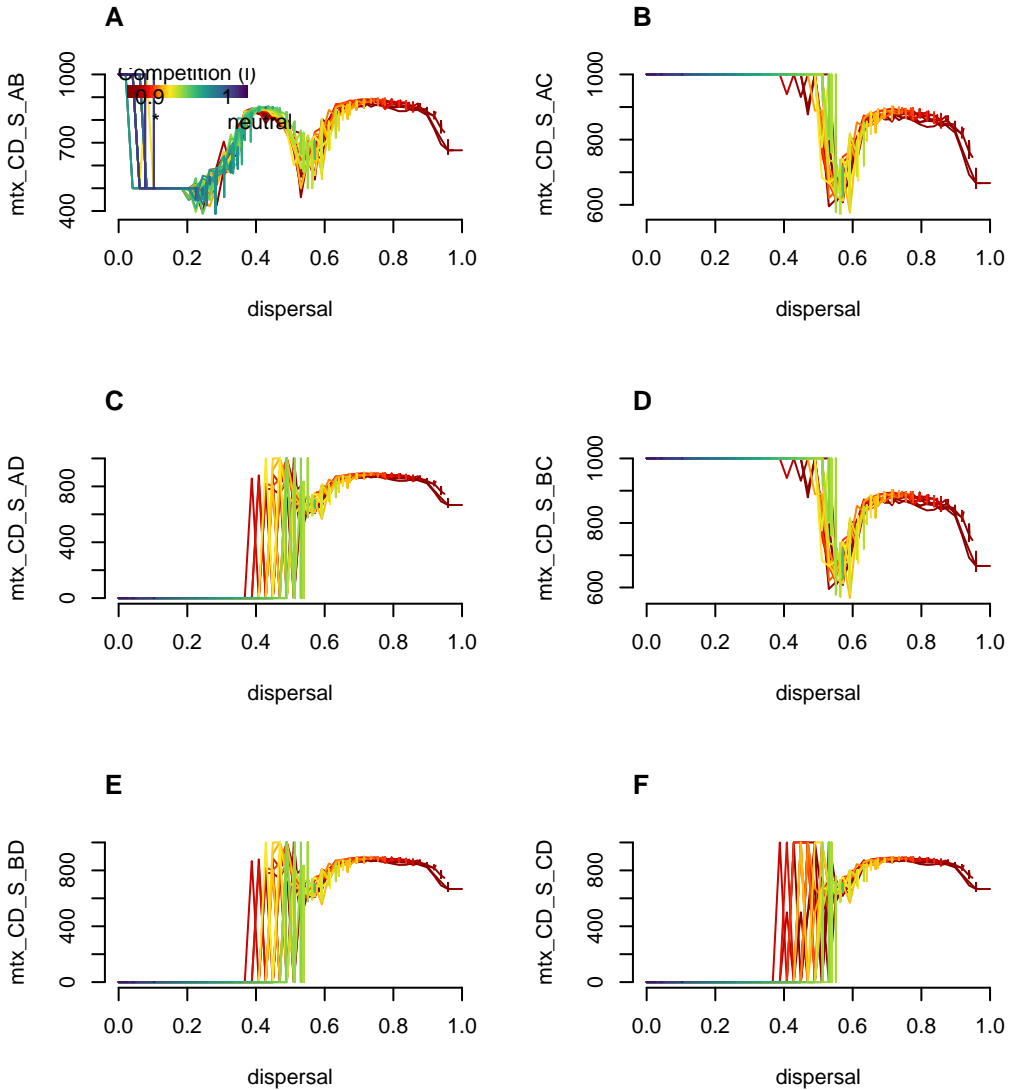


Figure 23: Community Distance between patches A, B, C and D for M0. Each line corresponds to simulations with a same competitive value.

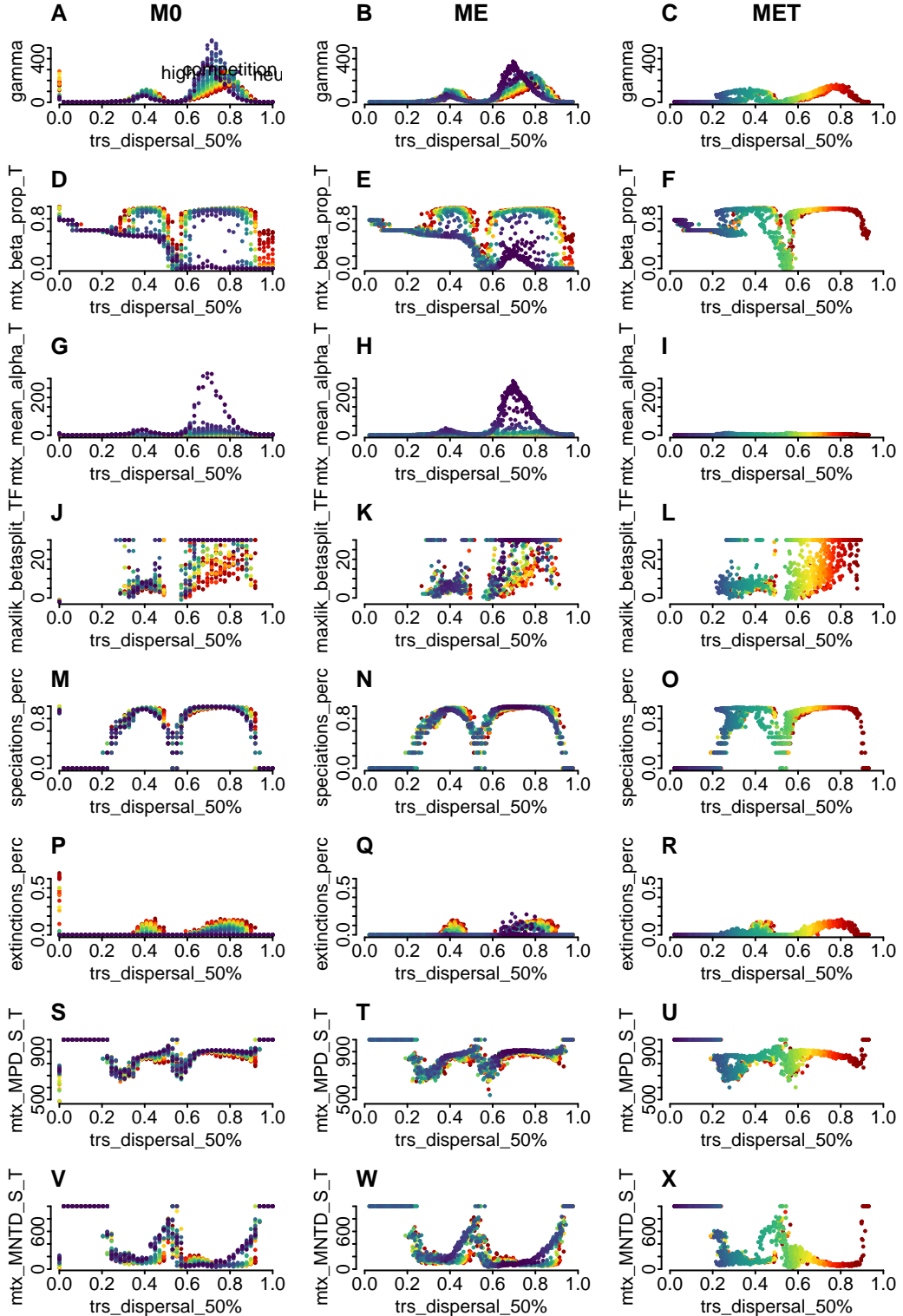


Figure 24: Comparison of M0, ME and MET for 8 summary statistics. Dispersal x axis is the mean dispersal trait at the end of the simulation, rather than the initial dispersal parameter. The same applies for the heterospecific tolerance that color the points

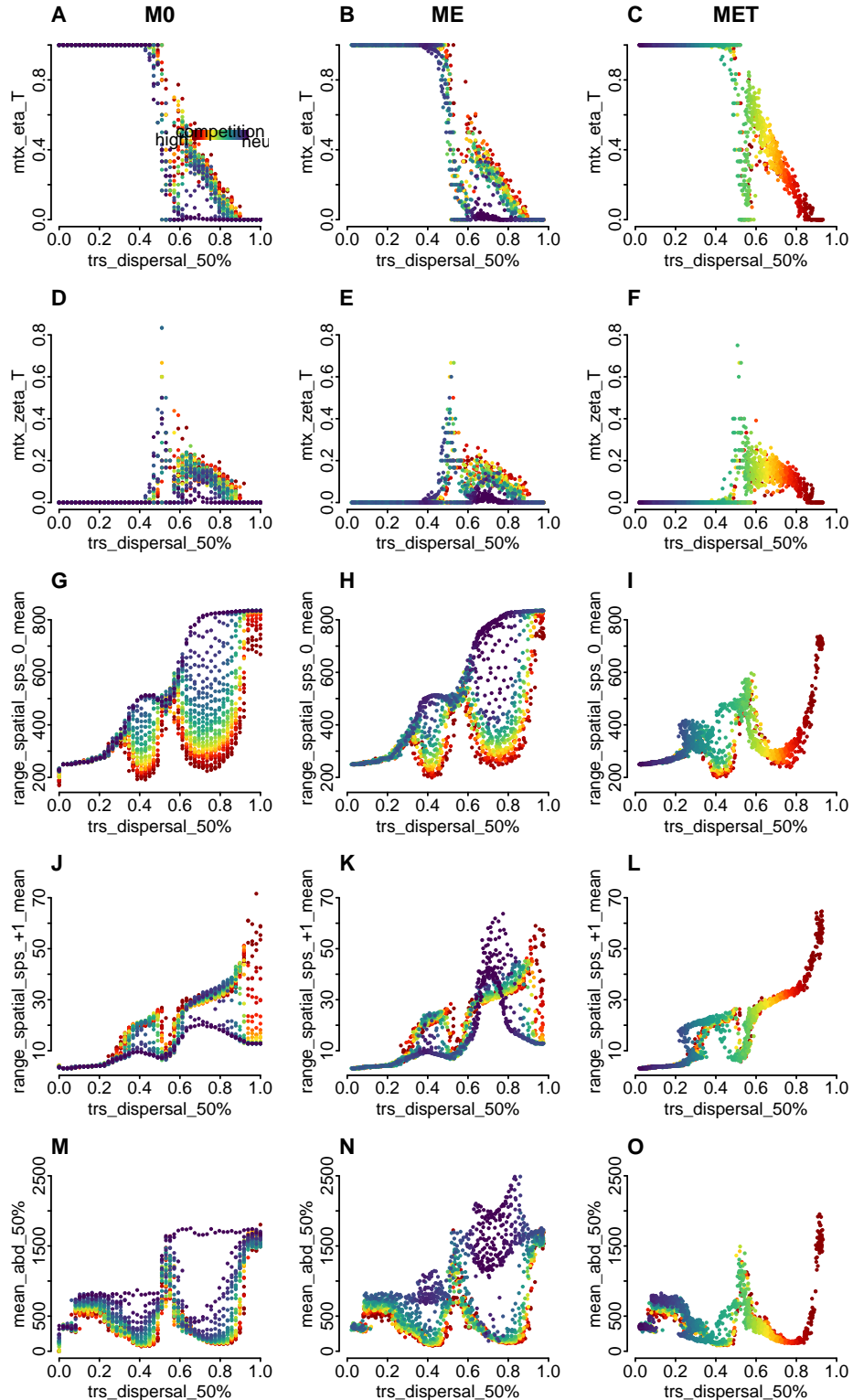


Figure 25: Comparison of M0, ME and MET for additional summary statistics. Dispersal x axis plot the mean dispersal trait at the end of the simulation, rather than the initial dispersal parameter. The same applies for the heterospecific tolerance that color the points.

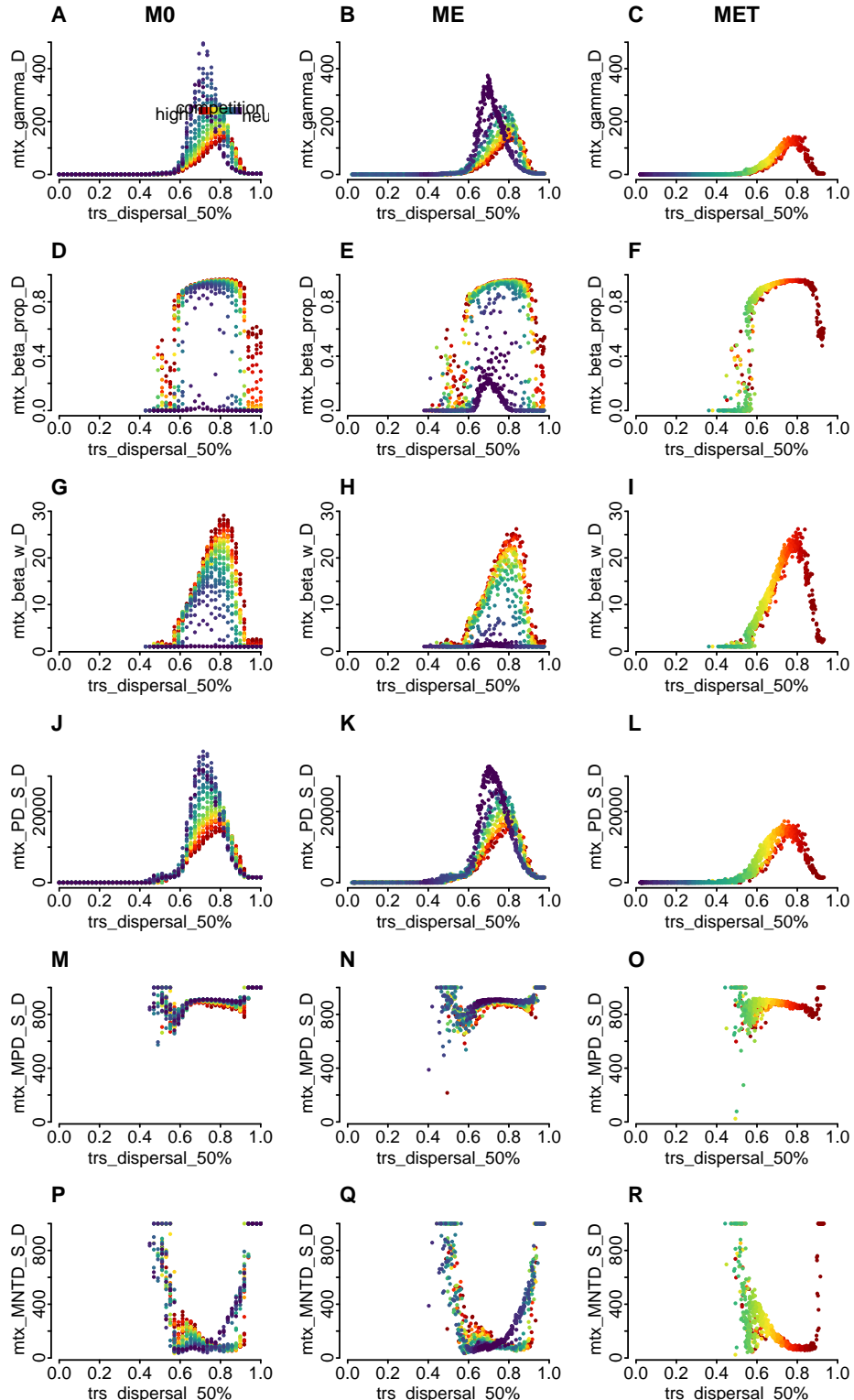


Figure 26: Comparison of M0, ME and MET for summary statistics related to patch D. Dispersal x axis plot the mean dispersal trait at the end of the simulation, rather than the initial dispersal parameter. The same applies for the heterospecific tolerance that color the points, i.e.

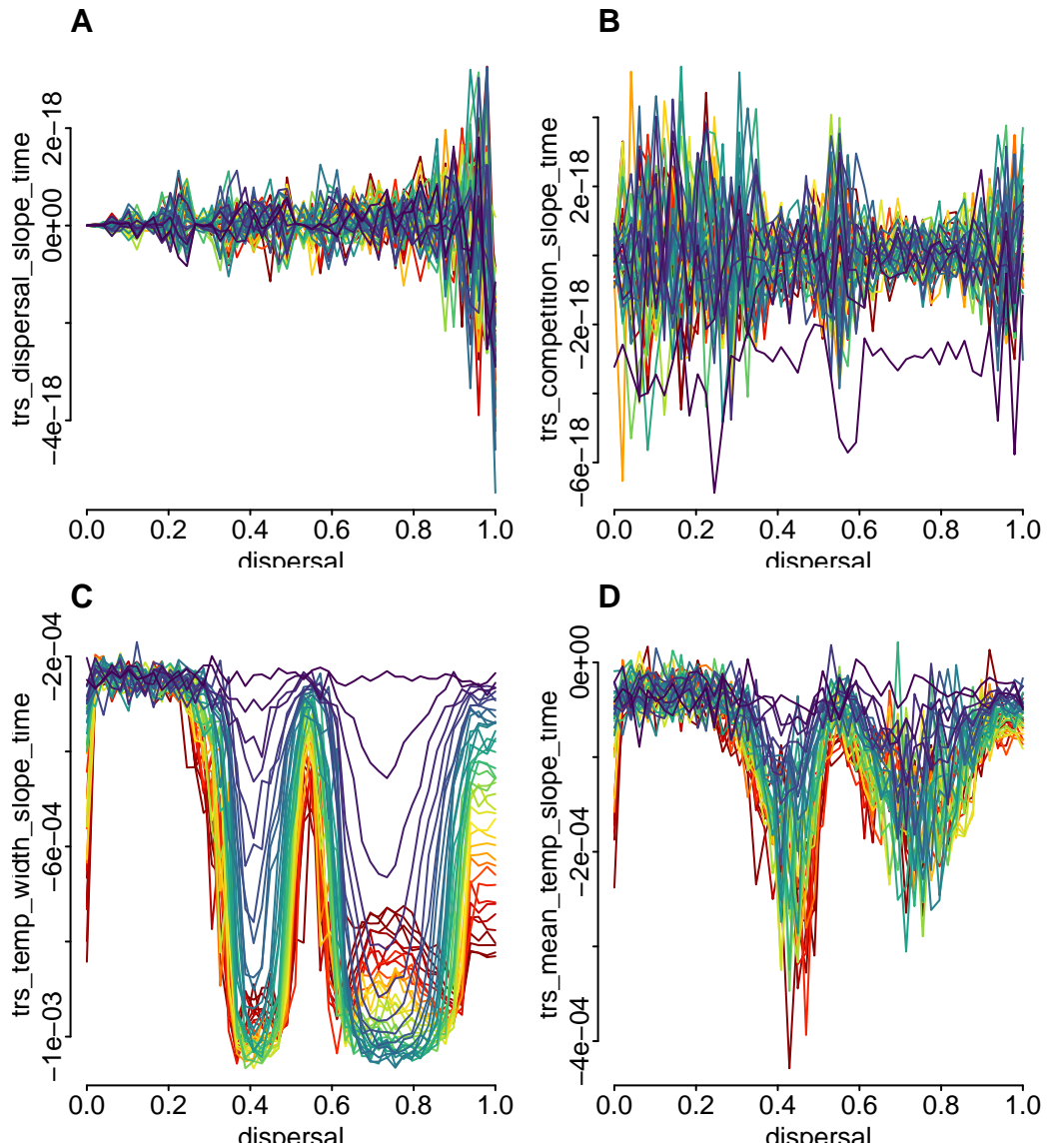


Figure 27: Model M0 slope of linear regression for entire time between dispersal (A), competition (B), temperature width (C) and mean temperature (D)

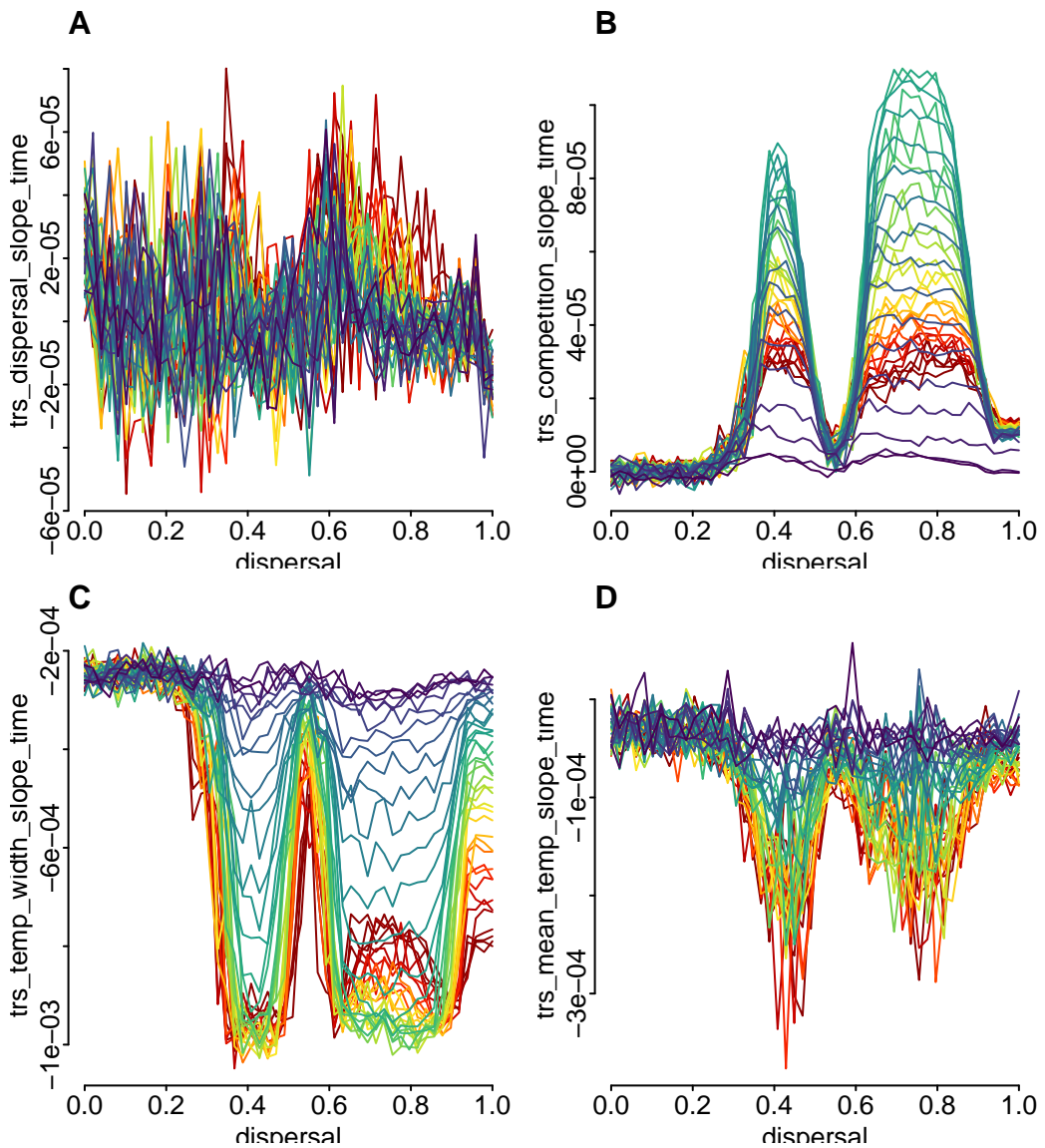


Figure 28: Model ME slope of linear regression for entire time between dispersal (A), competition (B), temperature width (C) and mean temperature (D)

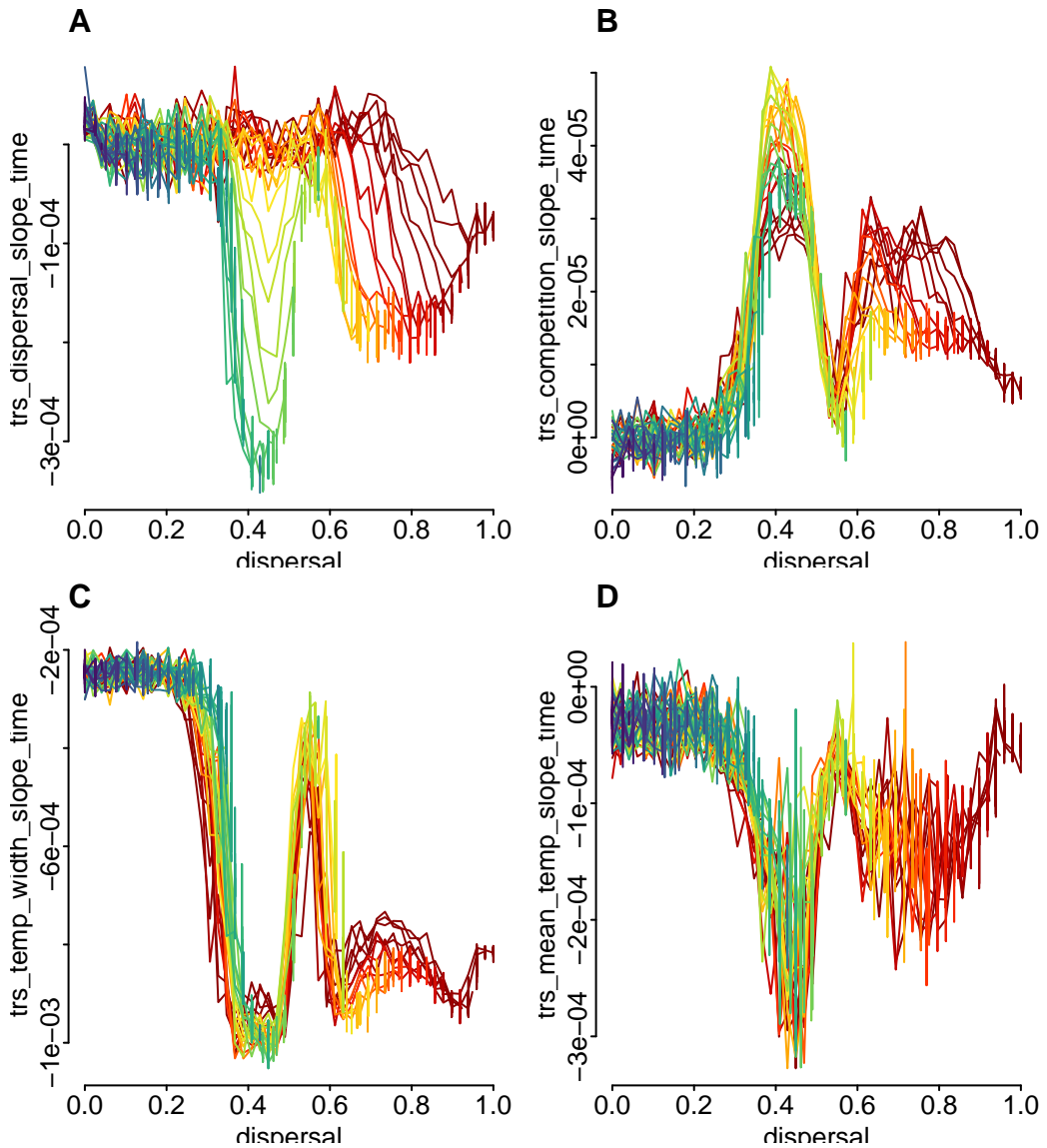


Figure 29: Model MET slope of linear regression for entire time between dispersal (A), competition (B), temperature width (C) and mean temperature (D)

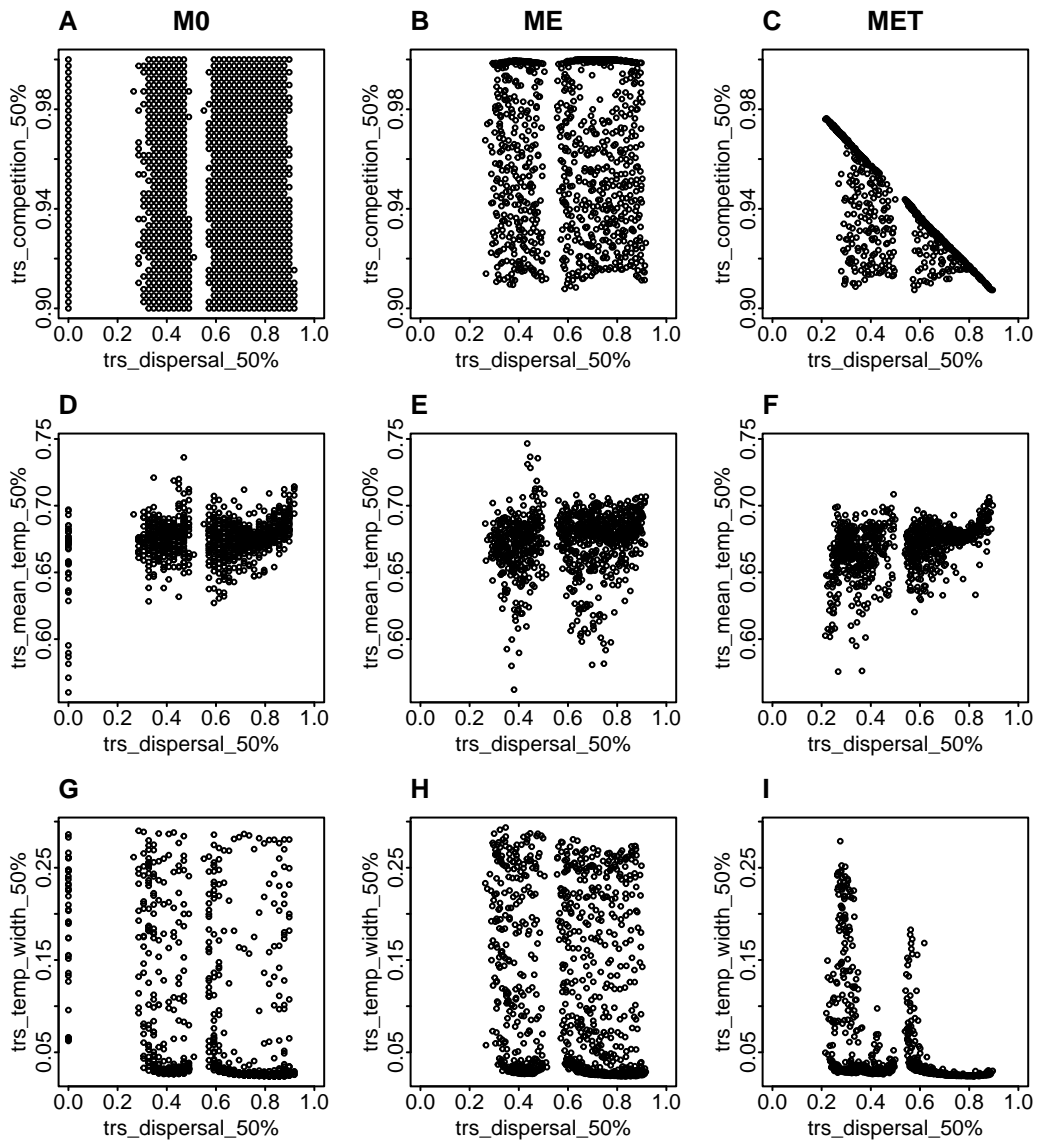


Figure 30: Final average competition, mean temp and niche width for M0 (A,D,G), ME (B,E,H) and MET (C, F, I).

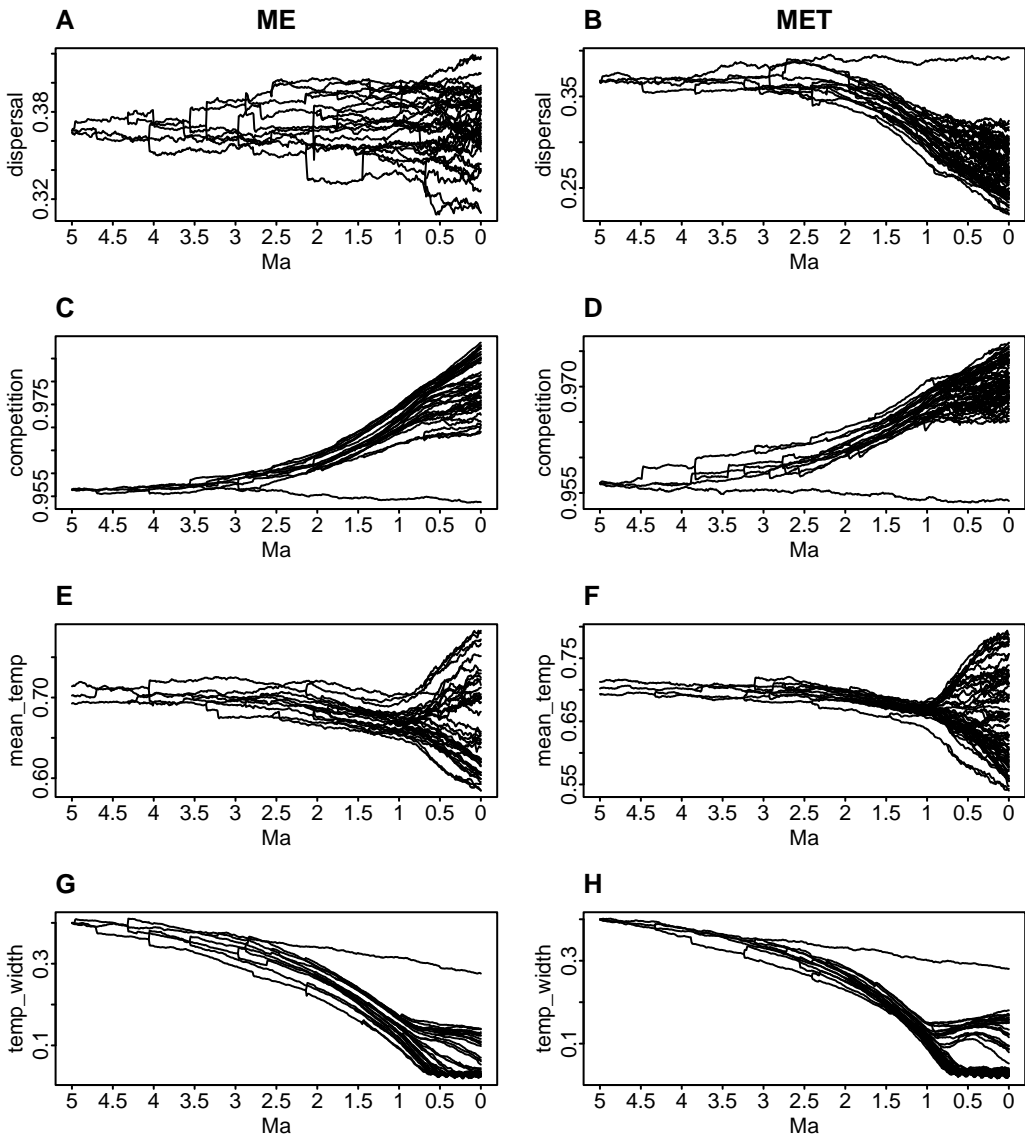


Figure 31: Phylogeny through time with y-axis showing mean trait value per species along time for dispersal (A,B), heterospecific tolerance (C,D), mean temperature (E,F) and temperature width (D,H) for a simulation (i.e. 1119) under ME and MET respectively. Config 1119 had uinitial dispersal = 0.367 and heterospecific tolerance = 0.956. Species 3 at patch C (outlier species at B, C, D, G, H) remained isolated throughout the simulation, which is indicated by the lack of evolution in heterospecific tolerance (C,D) since species 3 was not exposed to tinterspecific competition.

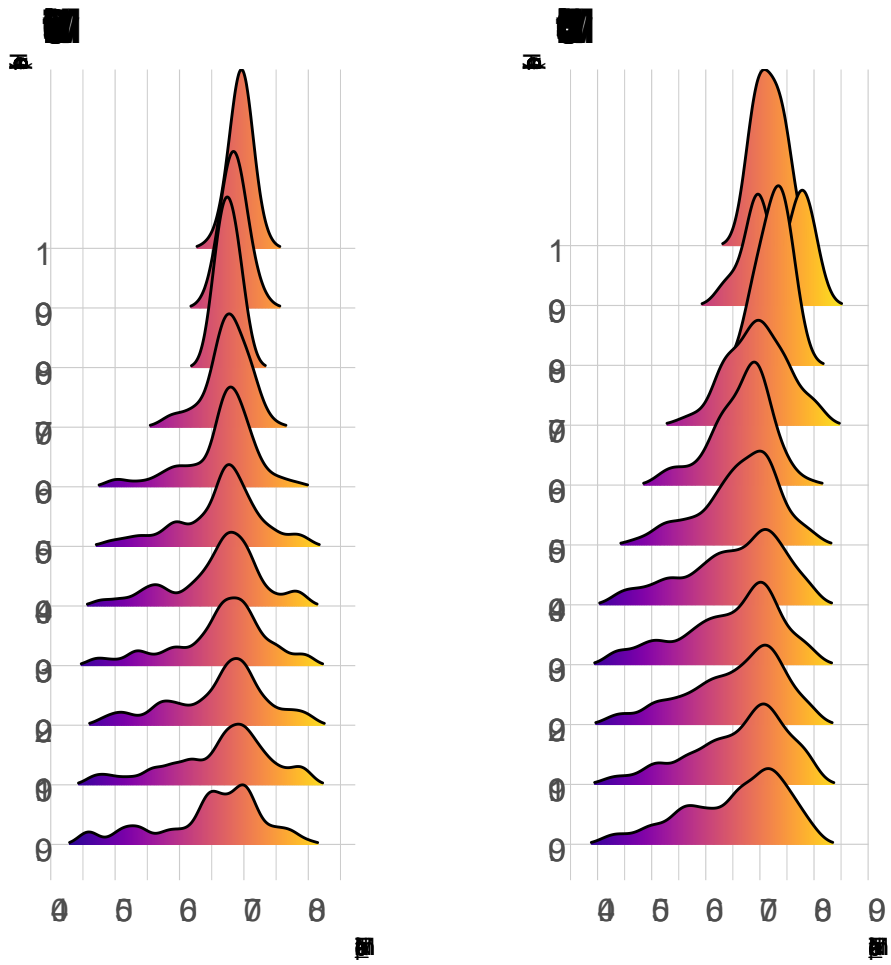


Figure 32: Ridgelineplots (density) of average mean temperature trait (T) for all the ancestor species at each speciation event over simulations with $d=0.3$ (A) and $d=0.45$ (B) across a gradient of heterospecific tolerance (colors correspond to the normalized mean temperature trait).

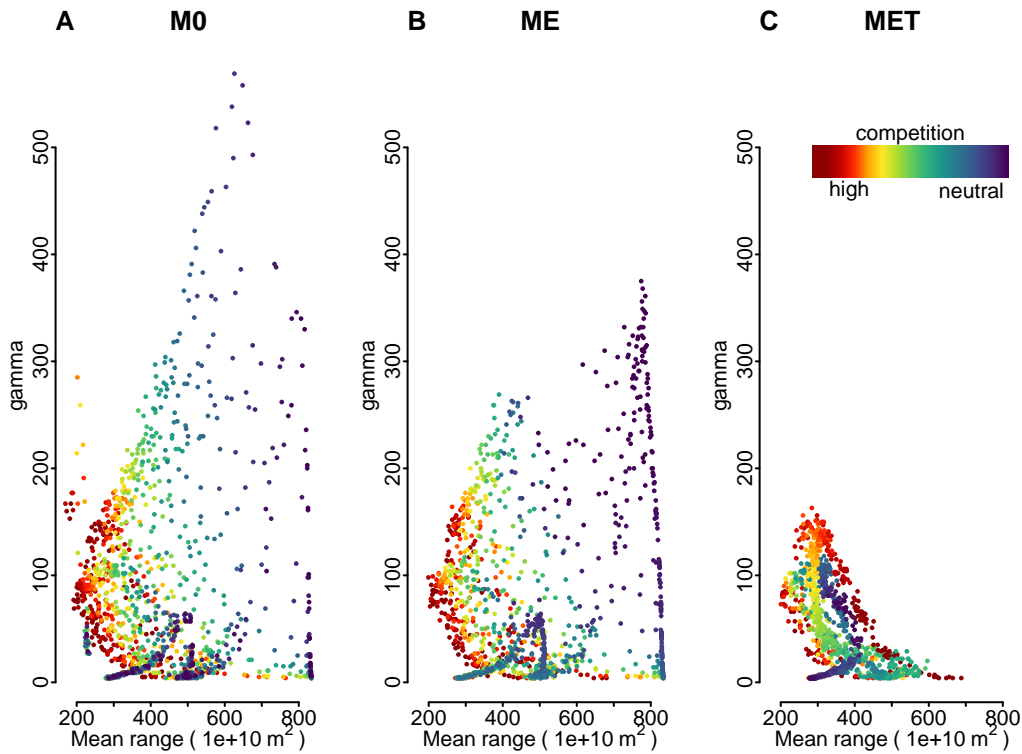


Figure 33: The theory of limiting similarity predicts that as species diversity increases, the average population size of each species decreases due to the need for coexisting species to be sufficiently different to coexist, resulting in lower population sizes with higher competition.

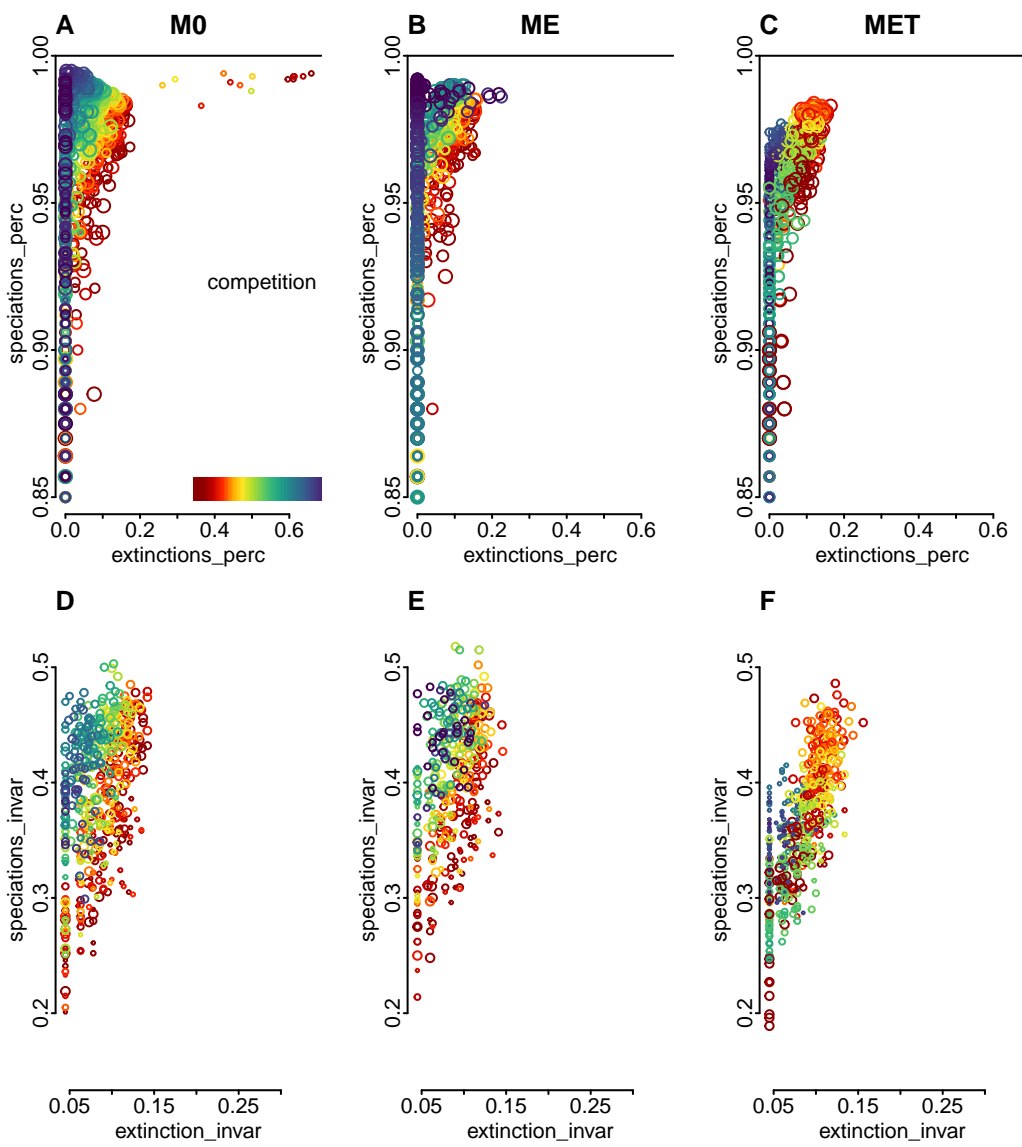


Figure 34: Speciation versus extinction percentage (A-C) and temporal invariability (i.e. temporal stability of macroevolutionary events) (D-F). MET was the only model that showed increased interspecific competition enhancing extinction and increasing speciation.

Earth's Climate and Its Predictability over the Last 66 Million Years." *Science* 369 (6509): 1383–87. <https://doi.org/10.1126/science.aba6853>.